





Energy dissipation of a carbon monoxide molecule manipulated using a metallic tip on copper surfaces

Norio Okabayashi ^{1,*}, Thomas Frederiksen ^{2,3,†}, Alexander Liebig ⁴, and Franz J. Giessibl ^{4,‡}

¹Graduate School of Natural Science and Technology, Kanazawa University, Ishikawa 920-1192, Japan

²Donostia International Physics Center (DIPC), San Sebastián 20018, Spain

³IKERBASQUE, Basque Foundation for Science, Bilbao 48013, Spain

⁴Institute of Experimental and Applied Physics, University of Regensburg, Regensburg D-93053, Germany



(Received 7 January 2023; revised 26 April 2023; accepted 24 May 2023; published 2 October 2023)

Friction is a familiar phenomenon to humankind and has long been studied; however, it is fundamentally difficult to understand because of the complex processes that contribute to it. For elucidating friction, it is helpful to simplify the system. In this respect, molecular manipulation, in which a single molecule or atom on a surface is moved by the tip of a scanning probe microscope, is an ideal research target. In this paper, we combine noncontact atomic force microscopy, inelastic electron tunneling spectroscopy, and density functional theory calculations to investigate the molecular manipulation process of a single CO molecule on Cu(110) and Cu(111) surfaces at low temperature. We discovered the presence of a metastable adsorption site that is not occupied when the tip is far from the surface but is engaged for close tip positions. This adsorption site plays the role of an intermediate state in the reaction path of manipulation, and this intermediate is important for understanding the dynamics of manipulation and dynamic friction. We elaborate the process leading to the above conclusions in detail and discuss future perspectives.

DOI: [10.1103/PhysRevB.108.165401](https://doi.org/10.1103/PhysRevB.108.165401)

I. INTRODUCTION

Friction occurs in the relative motion of two bodies in contact and is accompanied by energy dissipation [1]. The friction phenomena observed in macroscopic systems originate from complex processes at various length scales, making it difficult to understand these phenomena. Therefore, studies have focused on systems that are clearly defined at the atomic scale [1–5]. One example is the study of the processes by which molecules and atoms lose their translational kinetic energy through the creation of electron-hole pairs and of substrate phonons as they diffuse over or scatter at surfaces [6,7]. The loss of translational energy through vibrational excitation of surface molecules during scattering processes [8] and the subsequent relaxation of excited molecules by similar energy dissipation processes [9,10] have also been studied extensively.

Another example is the use of scanning tunneling microscopy (STM) and atomic force microscopy (AFM) [11,12]. AFM can provide a wealth of experimental data for understanding friction at the atomic level because it can measure the actual force between two objects and can limit the contact point to a single asperity [13–15]. The Prandtl–Tomlinson (PT) model has long been known as a model for understanding such nanoscale friction [16,17]. This theory is based on switching between metastable and stable states at bistable

potential energies and explains the phenomenon qualitatively well [18]. However, this model is too simplistic because it introduces empirical parameters that describe the potential between two objects. For a deeper understanding of friction, an interpretation based on *ab initio* calculations without empirical parameters is required.

These studies [13–15] were furthered using noncontact AFM [19], in which the contact point can be limited to the atomic level [20–22]. Noncontact AFM has the advantage that the dissipated energy can be evaluated from the power required to oscillate the cantilever at a constant amplitude [19]. Density functional theory (DFT) calculations for such noncontact conditions could reproduce switching with energy dissipation at a bistable potential as the oscillating tip approached the surface [23]. Further studies have been extended to the case of a single molecule confined between the tip and surface [24–26]. The key to this type of study is to identify the structure of the tip apex and adsorption state of the molecule. For the former, it has been reported that the structure of the tip apex can be determined by measuring the force mapping around an isolated CO molecule on the surface [19,27]. For the latter, inelastic electron tunneling spectroscopy (IETS) with AFM/STM [28–30] can be used to determine the adsorption site. Thus, by combining these two techniques, the contact point can be determined with unprecedented accuracy.

Significant progress has also been made in theoretical calculations to understand friction at the nanoscale [31,32]. It would be a major milestone if the experimental results of friction with precisely controlled contact points, such as those described above, could be reproduced by *ab initio* calculations. The progress of the theory necessary for such

*okabayashi@staff.kanazawa-u.ac.jp

†thomas_frederiksen@ehu.eus

‡franz.giessibl@ur.de

reproduction should not be overlooked. In this paper, we focus on a single CO molecule on a copper substrate, which is a standard system in surface science [33]. The top site is experimentally known to be the most stable adsorption site in this system; however, DFT calculations have long failed to reproduce this [34,35]. This suggests further difficulties if additional influences like the force exerted by the tip of a scanning probe microscope should be considered. Sixteen years ago, the deficiencies of local and semilocal exchange-correlation functionals for the adsorption problem was solved by considering more accurate quantum-chemistry treatments such as B3LYP and HF-MP2 for finite clusters [36]. A few years later, using the recently developed van der Waals (vdW) density-functionals (vdW-DF) [37–41], it was shown that inclusion of long-range dispersion forces can provide a correct description of the CO adsorption on metal surfaces [41], paving the way for describing extended systems in the spirit of DFT through the total electron density only.

Molecular manipulation by a probe tip [42–54] is representative of such research and is an ideal setting to investigate friction. This process is an essential technique for creating fascinating nanostructures on surfaces [55–57]; thus, its elemental processes have been intensively investigated [43–45]. In previous studies, the typical scenario was single hopping between two equivalent adsorption sites, as described in the PT model. The lateral force required to move an atom or a molecule on surfaces, i.e., the static frictional force, has also been measured using an AFM technique [46,48–54], and the results were interpreted based on this single-hopping scenario. However, discussion of the dynamics and energy dissipation in the manipulation process, i.e., dynamic friction, is lacking.

To address the dynamics of manipulation, we focus on the interaction between a single CO molecule adsorbed on a metal surface and a metal probe tip. The manipulation research for this system is not only related to the issue of friction but also to high-resolution imaging with a CO functionalized tip [27,58–65], manipulation through vibrational excitation by tunneling electrons [66–69], and force-induced chemical reactions by the probe tip [70–73].

Here, using noncontact AFM, STM-IETS, and state-of-the-art DFT calculations, we show that, when a metallic tip approaches a CO molecule on Cu(110) and Cu(111) surfaces, its adsorption state switches from the top site to a metastable adsorption site with energy dissipation [74]. Furthermore, we show that such a metastable site plays the role of an intermediate state in the reaction pathway of lateral manipulation of the CO molecule. We also demonstrate that it is possible to understand the molecular manipulation processes, including the distinction between static and dynamic frictional forces, by considering the contribution of such an intermediate state [74].

II. METHODS

A. Experimental

All measurements were performed at low temperature (4.4 K) under ultrahigh vacuum conditions using a combined STM and AFM system (LT-SPM by ScientaOmicron GmbH) at the University of Regensburg. The sample substrate was a Cu(110) or Cu(111) crystal, which was cleaned via repeated

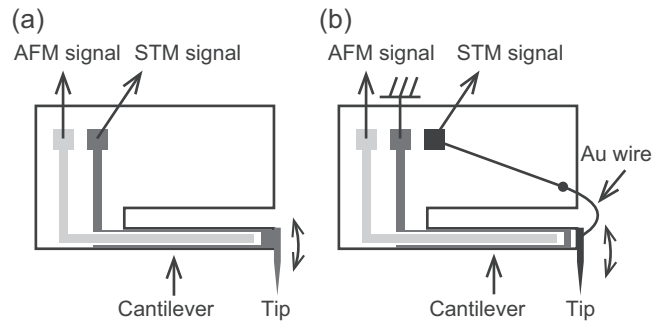


FIG. 1. Schematics of the two kinds of force sensors used in this study. (a) Force sensor with a simple structure suitable for a precise force measurement. (b) Force sensor with a gold wire suitable for high current measurement.

sputtering and annealing. CO molecules were then adsorbed on the surface at low temperature with a coverage of a few molecules per 10×10 nm area.

The force field was measured using a qPlus sensor [19,75], in which a metallic tip made of a tungsten wire with a diameter of $50 \mu\text{m}$ was attached to the sensor cantilever end (Fig. 1). For precise force and dissipation measurements, a sensor with a simple structure was used [Fig. 1(a)], in which a higher quality factor was available. In addition, the bias between the tip and sample was set to zero to minimize crosstalk. The parameters of this sensor were as follows: eigenfrequency $f_0 = 52\,194$ Hz, stiffness $k = 1800$ N/m, and quality factor $Q = 595\,000$. The frequency shift Δf of the vertically oscillating force sensor was measured at a constant amplitude $A = 20$ pm. In frequency-modulation AFM, the frequency shift of the sensor from its unperturbed resonant frequency is a measure of the vertical tip force gradient k_{ts} averaged over the sensor oscillation $\Delta f = f_0(k_{\text{ts}})/2k$ [19]. This force gradient was then converted into a force value and potential energy using a deconvolution method [76]. During the frequency-shift measurement, the excitation voltage V_{exc} added to the electrode of the piezo element to mechanically oscillate the cantilever at a constant amplitude was simultaneously measured, which was used to estimate the dissipation energy E_{dis} per oscillation cycle, using the following equation: $E_{\text{dis}} = 2\pi k A^2 / (2Q) \times V_{\text{exc}} / V_{\text{exc}0}$ [19], where $V_{\text{exc}0}$ is the excitation voltage when the tip is far away. The tip height $z = 0$ was chosen at the point contact, where the electrical conductance would reach the conductance quantum. When the tip oscillates, the distance between the lower turnaround point and $z = 0$ is defined as the tip height z_1 .

The tip attached to the cantilever was also used to measure the electron tunneling current, by which the IETS [28–30] curves were measured. In these measurements, a sensor with a gold wire [77,78] was used for current measurement [Fig. 1(b)] because the measurement of a high current under static conditions ($A = 0$ pm) is possible. In IETS, a modulation voltage of $V_{\text{mod}}^{\text{rms}} = 1.0$ mV was added to the sample bias, and the second-harmonic signal of the tunneling current was measured using a lock-in amplifier. We adopted radiofrequency (RF) filters to attenuate the RF noise from the environment, thus increasing the resolution of the IETS measurements [79]. For all AFM and STM-IETS

TABLE I. Investigation of the appropriate exchange-correlation functional to describe the interaction between a CO molecule and a Cu(110) surface. For each of the considered functionals, the computed lattice constant a_0 for the copper crystal is listed along with the corresponding adsorption energies for four adsorption sites of CO on Cu(110) (top, bridge, and low-top and low-bridge sites). The most stable configuration is highlighted in boldface. Consistent with Ref. [41], only the vdW-DF and vdW-DF2 functionals correctly predict that CO adsorbs on a top site, where the adsorption energies are close to the experimental value of 0.63 eV [94]. On the other hand, a_0 for these functionals are a bit larger than the experimental value of 360 pm, as discussed in Ref. [85].

Functional	a_0 (pm)	Top (eV)	Bridge (eV)	Low-top (eV)	Low-bridge (eV)
PBE	364	-0.918	-0.987	+0.053	+0.010
vdW-optB86b	360	-1.059	-1.142	-0.109	-0.128
vdW-DF (revPBE-vdW)	371	-0.681	-0.608	+0.045	-0.054
vdW-DF2 (rPW86-vdW2)	375	-0.627	-0.520	+0.063	-0.185

measurements, tips with apices consisting of a single atom [19,27] were used because (1) these tips can exert a stronger attractive force [80], which is preferable to induce manipulations in the lateral direction [49], and (2) these tips can provide stronger IETS signals [81].

B. DFT calculations

We computed the potential energy landscape, forces, and vibrational frequencies using periodic, plane-wave DFT calculations as implemented in VASP [82–84]. To correctly account for the preferred top-site adsorption of CO on Cu(110) and Cu(111) (Table I), we employed the vdW-DF2 non-local exchange-correlation functional [37–41]. Calculations were performed with the plane-wave energy cutoff set to 600 eV, a 4×4 Monkhorst-Pack k -point mesh, and first-order Methfessel-Paxton occupations with 0.1 eV smearing. The lattice constant for Cu was set to $a_0 = 375$ pm, as computed with the vdW-DF2 functional. As shown in Table I, the choice of the exchange-correlation functional shows the tradeoff relationship regarding the lattice constant and stable adsorption site. Note that this theoretical a_0 corresponds to the distance d between the nearest-neighboring Cu atoms of 265 pm, whereas the experimental a_0 of 360 pm [85] corresponds to $d = 255$ pm. Hereafter, $d = 265$ and 255 pm are adopted for the theoretical and experimental normalization of a lateral tip position, respectively.

The CO-Cu(110) system was represented in a 2×3 surface unit cell slab with 8 atomic layers and an ~ 2 -nm vacuum region between periodic images. Two models (Fig. 2) were explored for the tip apex geometry: a relatively inert Cu_{11} cluster and a more reactive Cu_5 cluster, with the relative coordinates fixed to those of the isolated cluster. The nominal height of the tip apex atom z_{cal} is measured from the point which is higher than the first layer of the copper substrate by 380 pm, which is close to the lattice constant: the definition is therefore like the experimental one. The geometry and total energy of the system were determined by relaxing CO and the topmost Cu layers (12 atoms/cell) for different tip positions (fixed supercell size) until residual forces on CO and the Cu surface layer were within 10^{-4} eV/pm. The Cu surface atoms away from the molecule were laterally constrained to avoid potential sliding effects of the top layer due to periodic boundary conditions. Background subtraction of the interaction energy was performed by also evaluating the total energy for supercells without CO. Harmonic vibrational

energies were computed by finite displacements with an amplitude of 5 pm, which provides good numerical accuracy to describe the low-frequency modes. The nudged elastic band (NEB) method [86] was used to compute reaction pathways, employing a two-stage approach with three intermediate images between end points at each stage.

III. RESULTS AND DISCUSSION

A. Lateral tip position-dependent manipulation

The lateral position of the tip relative to the CO molecule is important for varying the degree of interaction between CO and the tip. To determine the position of CO, we measured current images of CO molecules at a constant height on the Cu(110) surface, as shown in Fig. 3(a). The horizontal axis corresponds to the $[\bar{1}10]$ direction. The dip in the center of the image originates from the fact that the conductivity of CO is lower than that of the vacuum gap [87–90], and we can conclude that the top site is the center of the dip, as depicted by the red cross mark. Simultaneously with the tunneling current, a Δf image of CO was acquired [Fig. 3(b)], and a single dip due to the attractive interactions was observed

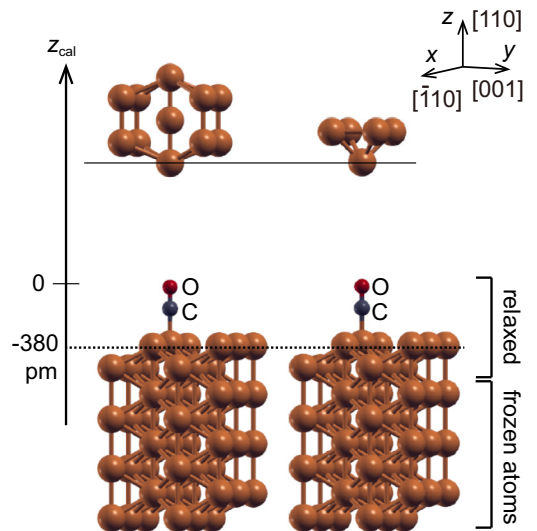


FIG. 2. Two tip structures over CO-Cu(110). Left: Cu_{11} tip. Right: Cu_5 tip. As shown in Fig. 5, the Cu_5 tip is about two times as reactive as the Cu_{11} tip.

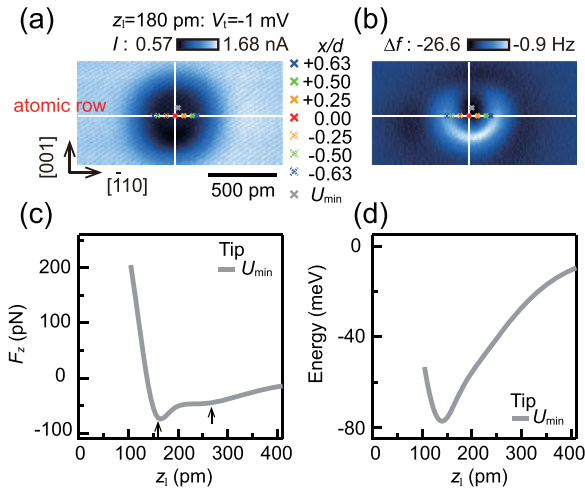


FIG. 3. Characterization of the tip apex and tip position. (a) Constant height current image of a CO molecule on a Cu(110) surface that was measured at a sample bias of -1 mV and a tip height of $z_1 = 180$ pm. (b) Constant height Δf image above the CO molecule acquired simultaneously with (a). (c) Short-range vertical force F_z and (d) potential energy for the tip laterally positioned over the potential minimum U_{\min} [gray cross in (a,b)], where the background component for the tip on the Cu surface has been subtracted.

around the CO molecule. This dip indicates that the tip apex is composed of a single atom [19,27]. The lateral tip position at which Δf reaches a minimum (U_{\min} : gray cross mark) is slightly displaced from the top site owing to the tip asymmetry including its tilt. The short-range vertical force F_z and potential energy at this potential minimum are plotted as functions of the tip height in Figs. 3(c) and 3(d), respectively. The two components of the F_z curve, indicated by arrows, correspond to vdW and chemical interactions [64].

The interaction between the tip and CO was further investigated experimentally by varying the tip position. In Figs. 3(a) and 3(b), the tip position x divided by the distance d between the nearest-neighboring Cu atoms is indicated along with the cross marks: $x/d = 0$ (top site), ± 0.25 (midpoint between the top and bridge site), ± 0.5 (bridge site), and ± 0.63 (beyond the bridge site). The Δf curves for each location are plotted in Fig. 4(a) as a function of tip height, with the cases of the tip approach and retraction depicted by solid and dotted lines, respectively. In all the cases, Δf first decreases and then increases as the tip approaches. When the tip is brought even closer, differences become visible. When the tip is inside the bridge site ($x/d = 0, \pm 0.25$), there is a sharp decrease in Δf as indicated by the black arrows, which corresponds to CO manipulation between the top and bridge sites, as explained later. In these cases, the Δf curves between the tip approach and retraction are identical at all z positions.

However, when the tip is beyond the bridge site ($x/d = \pm 0.63$), the situation changes. A significant difference is observed in the Δf curves between the tip approach and retraction. In these cases, STM images confirmed that the CO adsorption site after tip retraction is the neighboring top site [see the inset of Fig. 4(a) for $x/d = +0.5$]. Thus, we conclude that the change in the Δf curves at the gray arrows

in Fig. 4(a) correspond to the manipulation from one top to the neighboring top site. Note that, once the manipulation to the neighboring top site occurs, the situation becomes like the case of the tip inside the bridge site. Indeed, for further approaching the tip, Δf decreases abruptly, as shown by the black arrow. The Δf curves for the tip approach cases in Fig. 4(a) are converted to F_z in Fig. 4(b) and potential energy in Fig. 4(c) up to the tip height at which manipulation occurred. In these measurements of the Δf curves, the energy dissipation signal was also measured [Fig. 4(d)]. A pronounced energy dissipation signal is observed when manipulations of CO occur between the top and bridge sites (black arrows for $x/d = 0, \pm 0.25, -0.5$) and between the neighboring top and bridge sites (black arrows for $x/d = +0.5, \pm 0.63$). However, this is not the case for manipulations from the top to the neighboring top site (gray arrows for $x/d = +0.5, \pm 0.63$). One feature of the dissipation signal between the top and bridge sites is that its onset occurs at larger tip heights when the lateral tip position changes from the top toward the bridge (red, orange, and green curves).

These results can be interpreted using DFT calculations. Figure 5 shows the results of calculations of the potential energy between the Cu tip and CO on the Cu(110) surface [Fig. 5(a) for the Cu_{11} tip and Fig. 5(b) for the Cu_5 tip]. In each panel, the black, red, and blue lines represent the adsorption of CO on the top (T), bridge (B), and neighboring top (NT) sites, respectively. For both tip structures, the lateral tip position is systematically changed from $x/d = 0$ to 0.5, and extended to 1.0 due to mirror symmetry around $x/d = 0.5$. Notably, the potential energies between T and NT are symmetric with respect to the tip position at the bridge site; for example, the potential energy for T at $x/d = 0.2$ is the same as the potential energy for NT at $x/d = 0.8$. For both tip structures, the top site is most stable when the tip is inside the bridge site ($x/d < 0.5$) and the tip is far away. When the tip is very close to the surface, the bridge site becomes most stable. This crossover from T to B [see the arrows in Fig. 5(a) for the case of $x/d = 0.3$ with the Cu_{11} tip] is the origin of the steep decrease in the Δf curves in Fig. 4(a) ($x/d = 0, \pm 0.25, -0.5$).

In contrast, if the tip is beyond the bridge site ($x/d > 0.5$), the neighboring top site is most stable. However, this transition from the top to the neighboring top site is prevented by the presence of a barrier in the reaction pathway, the height of which is approximately determined by the energy of CO on the bridge site, as explained later. In this case, when the tip gets close enough to CO, manipulation to the bridge site occurs first, followed by manipulation to the neighboring top site, as indicated by the arrows in Fig. 5(a) for $x/d = 0.8$ with the Cu_{11} tip. This difference in the manipulation process depending on the lateral tip position is consistent with the observations in Fig. 4(a). Moreover, the tip height z_{cross} , in which the potential energies for the top and bridge cross each other, increases with the lateral tip position moving from the top ($x/d = 0$) to the bridge site ($x/d = 0.5$), as shown in Fig. 6, which is consistent with the experimental observations of the onset of dissipation in Fig. 4(d).

To understand the origin of the appearance of the dissipation signal for the manipulation processes, we investigated the energy of CO along the reaction path from the top to the neigh-

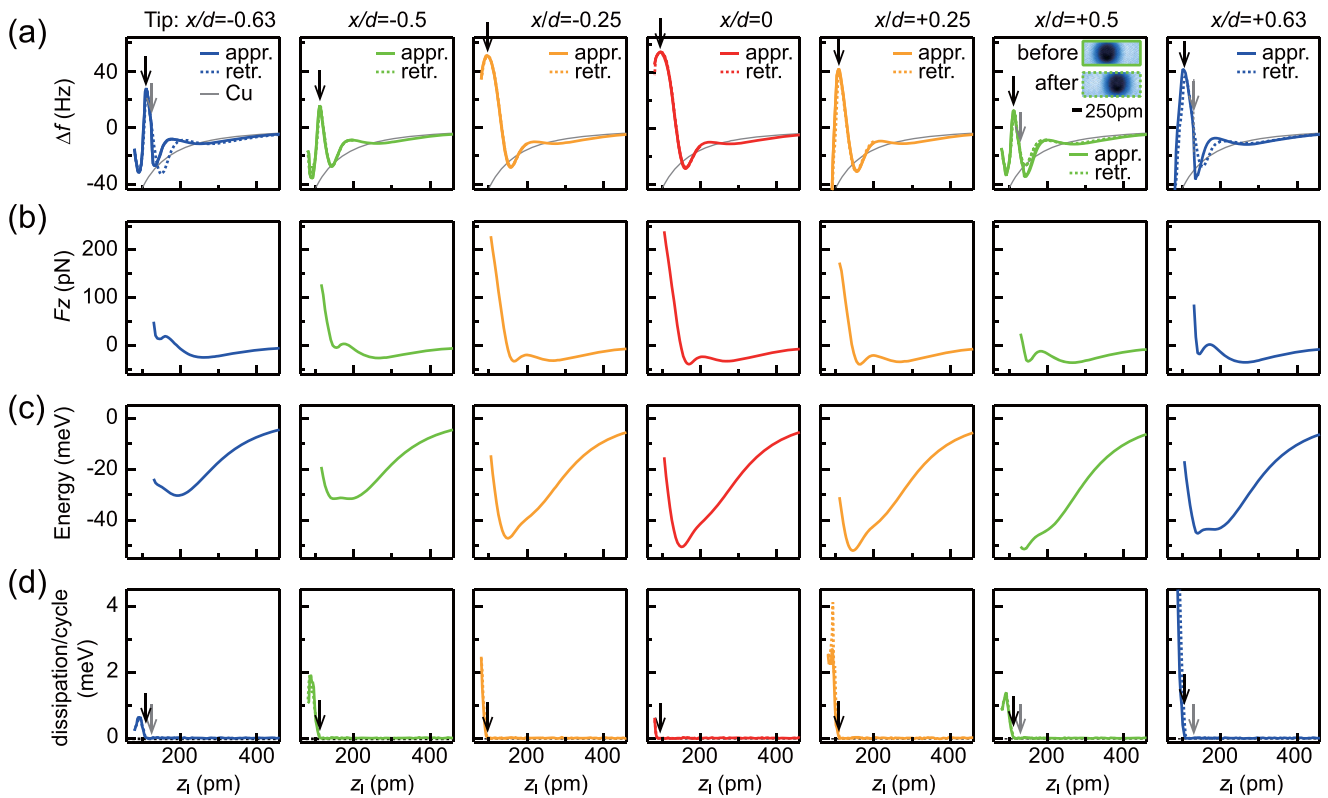


FIG. 4. Experimental results of tip-height-dependent atomic force microscopy (AFM) measurements for seven lateral tip positions ranging from $x/d = -0.63$ to 0.63 at the cross marks indicated in Figs. 3(a) and 3(b). (a) Frequency shift, (b) vertical force, (c) potential energy, and (d) dissipation/cycle (no background subtraction). In these measurements, the bias is set to be zero to avoid the crosstalk. (a) shows the case for both tip approach and retraction. In addition, the case for the tip on the Cu surface is also shown by a gray line. The difference in Δf between on CO and on Cu is very small at the maximum tip height in the figure (460 pm), which becomes negligible at the farthest tip position of the measurement of $z = 1$ nm. Also, in (a), at $x/d = +0.5, \pm 0.63$, the discontinuous change in Δf was observed, as shown by the gray arrow, where the manipulation from the top to the neighboring top site occurs. The manipulation could be confirmed by observing the image of the CO molecule before and after a set of tip approach and retraction, as shown in the inset for $x/d = +0.5$. In (b) and (c), the vertical force and potential energy are plotted until the manipulation occurs between the top and bridge sites for $x/d = 0, \pm 0.25$, and -0.5 and between the top and neighboring top sites for $x/d = +0.5, \pm 0.63$. (d) shows the dissipation per cycle for the tip approach and retraction. The background dissipation signal was extremely small ($24 \mu\text{eV}/\text{cycle}$) due to the very high Q condition ($Q = 595\,000$). The dissipation signal was nearly constant from the far position to the z position, where the strong dissipation signal begins to be observed. This constant dissipation proves that the crosstalk can indeed be ignored.

boring top site (Fig. 7 for the Cu_{11} tip, Fig. 8 for the Cu_5 tip), where the lateral tip position was systematically changed. In each panel, the cross marks in the left- and rightmost regions correspond to CO on the top and neighboring top sites, respectively. Moreover, the cross mark at the center corresponds to CO on the bridge site, which indicates that manipulation occurs through the bridge site. When the tip is inside the bridge site ($x/d < 0.5$), CO on the top site is most stable for the far tip position ($z_{\text{cal}} = 200$ pm). Because the manipulation process during tip approach/retraction is essentially the same for these tip locations ($x/d < 0.5$), we will specifically select the case of $x/d = 0.3$ with the Cu_{11} tip (Fig. 7) for the following discussion. In this case, as the tip approaches $z_{\text{cal}} = 125$ pm, the energies of CO on the top and bridge become comparable; however, spontaneous transitions are prevented owing to the presence of a barrier along the reaction path. It should be noted that, in our experiment, the sensor oscillated with a peak-to-peak amplitude of $2A = 40$ pm between its lower and upper turnaround points. When the tip oscillates around $z_{\text{cal}} = 125$ pm, the barrier disappears near the lower

turnaround point (e.g., $z_{\text{cal}} = 110$ pm), resulting in a transition to the bridge site. Conversely, when the tip retracts from the surface to the upper turnaround point (e.g., $z_{\text{cal}} = 140$ pm), CO on the top site becomes stable again. However, a small energy barrier remains between these two states, preventing the spontaneous transition of CO back to the top site. Assuming that the height of a barrier is ~ 10 meV from $z = 135$ to 145 pm, the period of an oscillation is $19 \mu\text{s}$, the attempt rate of a laterally vibrated CO molecule is 1 THz ($\sim 4 \text{ meV}$), and the temperature is 4.4 K , the transition probability is estimated by the Arrhenius equation to be $\sim 2 \times 10^{-5}$ for one oscillation cycle. This is very sensitive to the actual barrier height; in any case, we can expect the CO molecule to return to the top site around the upper turnaround point of the tip. The above discussion means that the tip height at which a manipulation occurs is different between the tip approach and retraction, which is the origin of a hysteresis essential for the observation of energy dissipation.

When the transition from a metastable state to a stable state occurs, the CO molecule is initially vibrationally

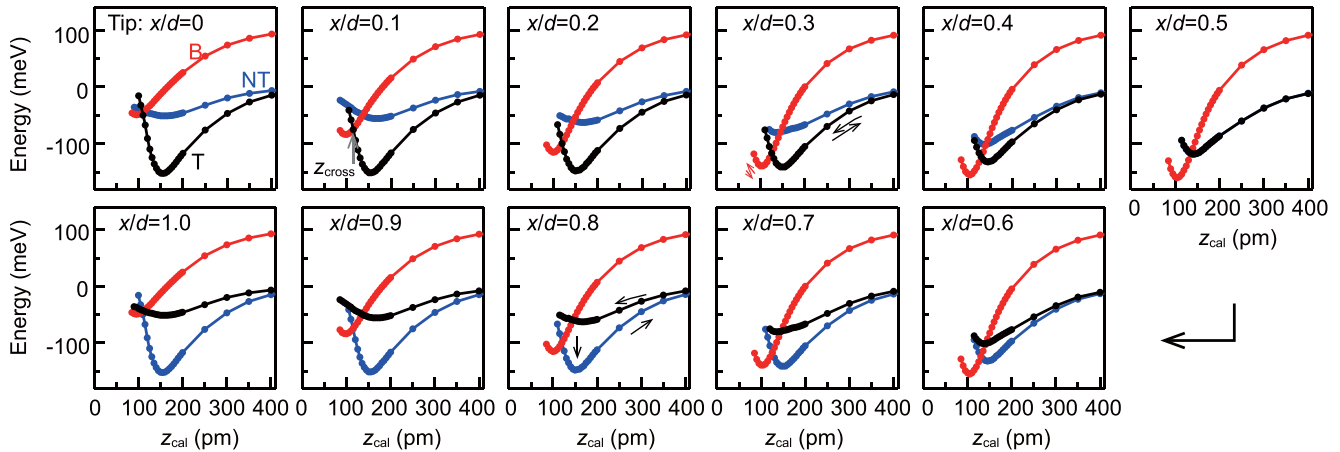
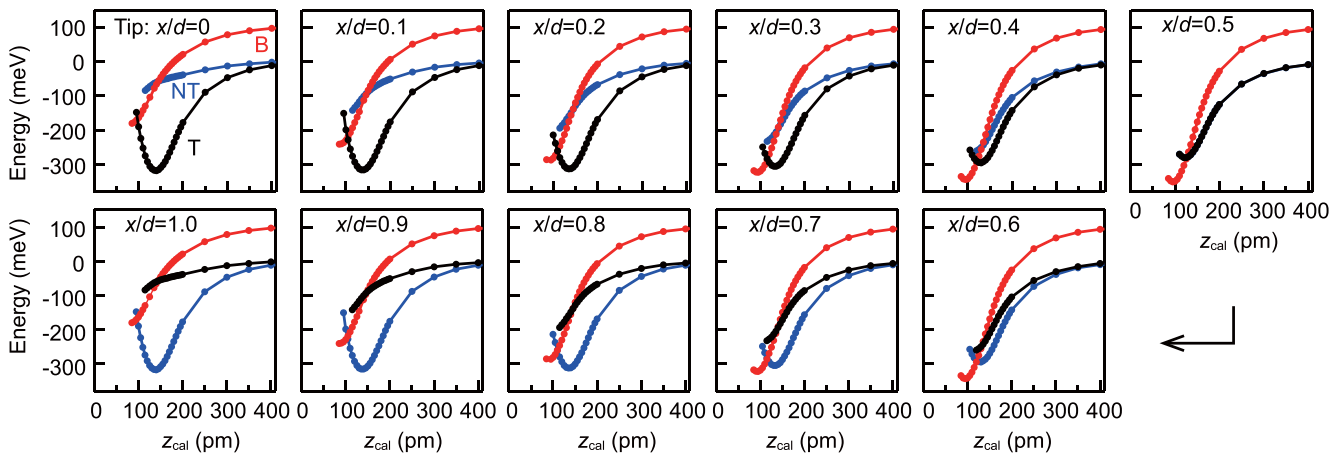
(a) Cu₁₁ Tip(b) Cu₅ Tip

FIG. 5. Theoretical investigation of the tip-height-dependent potential energies between a CO molecule on a Cu(110) surface and a Cu tip. (a) The cases for the inert Cu₁₁ tip are shown, where the lateral tip position is systematically changed. In each panel, the black, red, and blue lines represent the adsorption of CO on the top (T), bridge (B), and neighboring top (NT) site, respectively. (b) Like in (a) but for the case of the more reactive Cu₅ tip. Note that the Cu₁₁ tip is more realistic in the sense that the maximum absolute value of the potential energy in the experiment is 77 meV [Fig. 3(c)], while those of the Cu₁₁ and Cu₅ tips for $x/d = 0$ are 152 and 318 meV, respectively.

excited on the stable adsorption site and then decays into the vibrational ground state by generating electron-hole pairs in

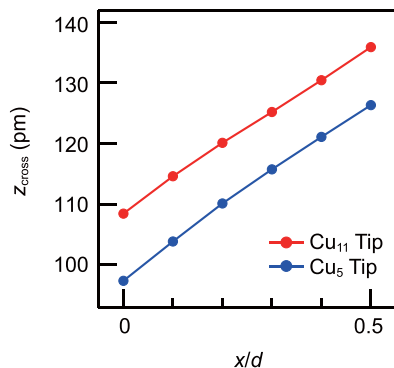


FIG. 6. Tip height z_{cross} , where the potential energies for CO on top and bridge sites in Fig. 5 become identical [see the arrow in Fig. 5(a) for the case of $x/d = 0.1$] are plotted as a function of lateral tip position.

the metal or substrate phonons. The lifetime of these decay processes at a metal surface has been estimated to be of the order of a few picoseconds for both stretching and bending modes [9,10], which is negligible compared with the cycle of the cantilever (19 μs). Therefore, it is reasonable to assume that the dissipation process occurs immediately after CO manipulation.

For tip positions beyond the bridge site ($x/d > 0.5$), the situation changes significantly, where the CO on the neighboring top site is already most stable, even at the far tip position ($z_{\text{cal}} = 200$ pm). However, no transition occurs because a barrier exists in the reaction pathway, the height of which is determined by the energy of the bridge site. In the following, we specifically choose the case of $x/d = 0.8$ with the Cu₁₁ tip (Fig. 7) to explain the process in detail. In this case, when the lower turnaround point of the oscillated tip reaches $z_{\text{cal}} = 125$ pm, CO is first manipulated to the bridge site, as in the case of a tip located inside the bridge site. As the tip retracts from the lower turnaround point to the

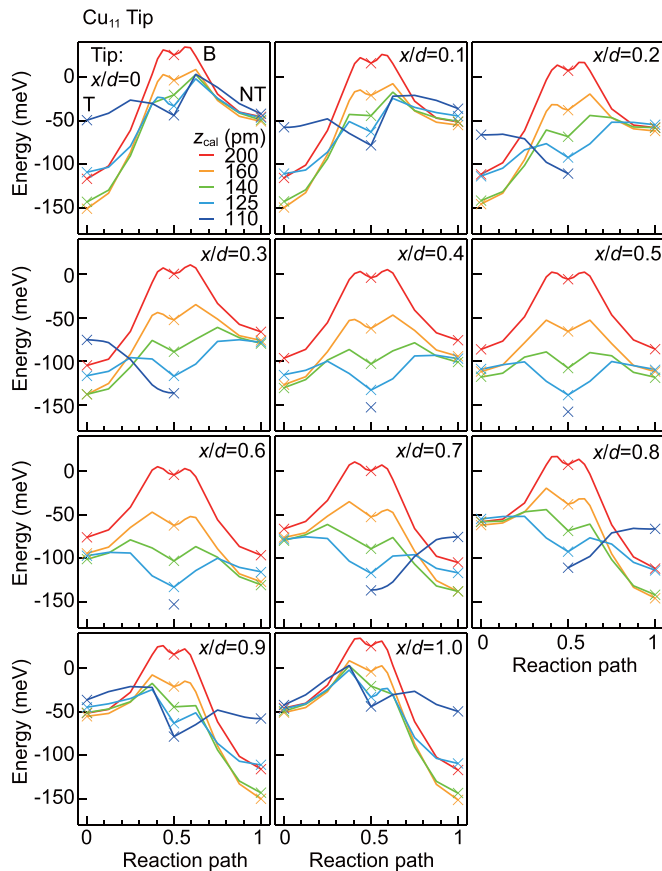


FIG. 7. Calculated nudged elastic band (NEB) reaction pathways for CO on Cu(110) from the top site (0.0) to the next top site (1.0) via bridge site (0.5) for fixed Cu₁₁ tip position. In each panel, the left- and rightmost points highlighted by the cross marks correspond to the CO molecule on the top site and that on the neighboring top site, respectively. The cross marks between these two points correspond to the CO molecule on the bridge site.

upper turnaround (e.g., $z_{\text{cal}} = 160$ pm), the barrier for the transition from the bridge to the neighboring top becomes so small that the CO molecule can eventually be manipulated to the neighboring top site after repeated tip oscillations. This transition occurs only once, even though the tip repeatedly approaches and retracts, because CO on the neighboring top site is most stable. In this case, no energy dissipation signal can be detected in the time-averaged experiment.

B. IETS

This scenario of CO manipulation from the top to the bridge was further investigated by adding IETS to the force and dissipation measurements [30]. Figure 9(a) shows the tunneling current on the CO molecule (black) and on the Cu substrate (gray) as a function of the tip height. At $z = 0$ pm, the extrapolated current (dotted line) on the Cu substrate corresponds to the quantum of conductance. When the metallic tip approaches the CO molecule from a distance, the tunneling current increases exponentially, as represented by the black line, and this increase in the current is enhanced at $z = 71$ pm (green line). This enhancement is consistent with the transition of CO from the top to the bridge site because

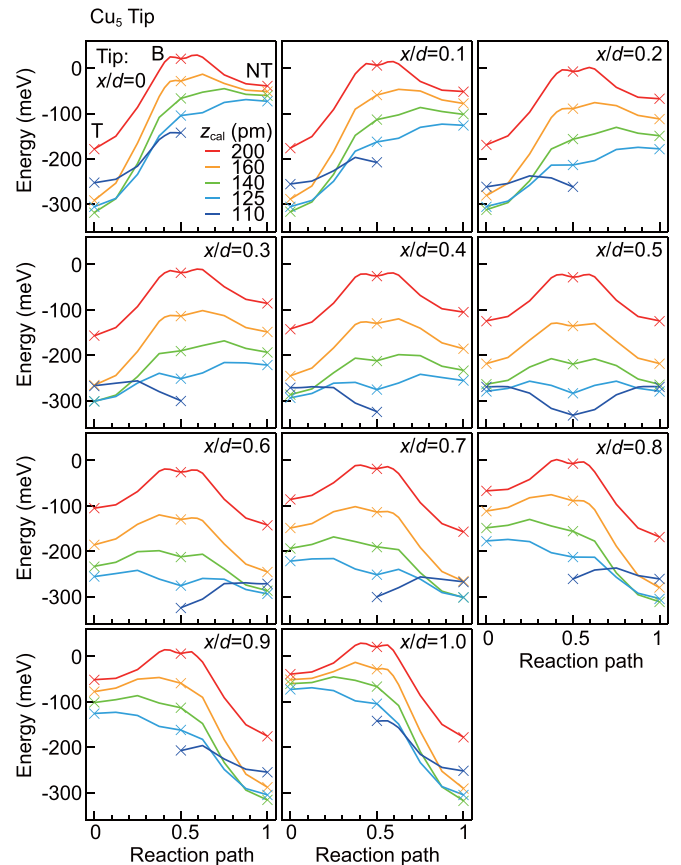


FIG. 8. Calculated nudged elastic band (NEB) reaction pathways for CO on Cu(110) from the top site (0.0) to the next top site (1.0) via bridge site (0.5) for fixed Cu₅ tip position. This case is like that shown in Fig. 7 but for the Cu₅ tip.

CO on the copper surface is less conductive than the vacuum gap [87–90]. Figure 9(b) plots the short-range vertical force as a function of tip height; as in Fig. 4, when the distance between the tip and molecule decreases to below $z = 75$ pm, there is a significant decrease in the force curve and a dissipation signal (not shown here).

The change in the adsorption sites can be confirmed from the vibrational energy shifts. Figure 9(c) shows the IETS dataset dependent on the tip height for a CO-Cu(110) surface, where the tip was located on a CO molecule. For $z = 280$ – 80 pm, each IETS curve consistently consists of two components of the frustrated translational (FT, 4–7 meV) and frustrated rotational (FR, 34–35 meV) modes, although their energies change significantly owing to the force from the tip [29,30]. The IETS curve changes significantly when the tip approaches $z = 70$ pm. A feature centered at 13 mV is seen (represented by green arrows), depicting a structure resembling the derivative of a Lorentzian. Furthermore, a normal inelastic signal is seen at ~ 34 mV (indicated by red arrows). When the tip further approaches $z = 60$ pm, this feature of the derivative of a Lorentzian disappears, and only the normal inelastic signals are seen at 8.3, 13.6, 18.5, and 36.2 mV (represented by blue arrows), consistent with the scenario of the adsorption site change.

Figures 9(d) and 9(e) show the bias-dependent (d) current and (e) conductance (dI/dV) for the CO molecule on the

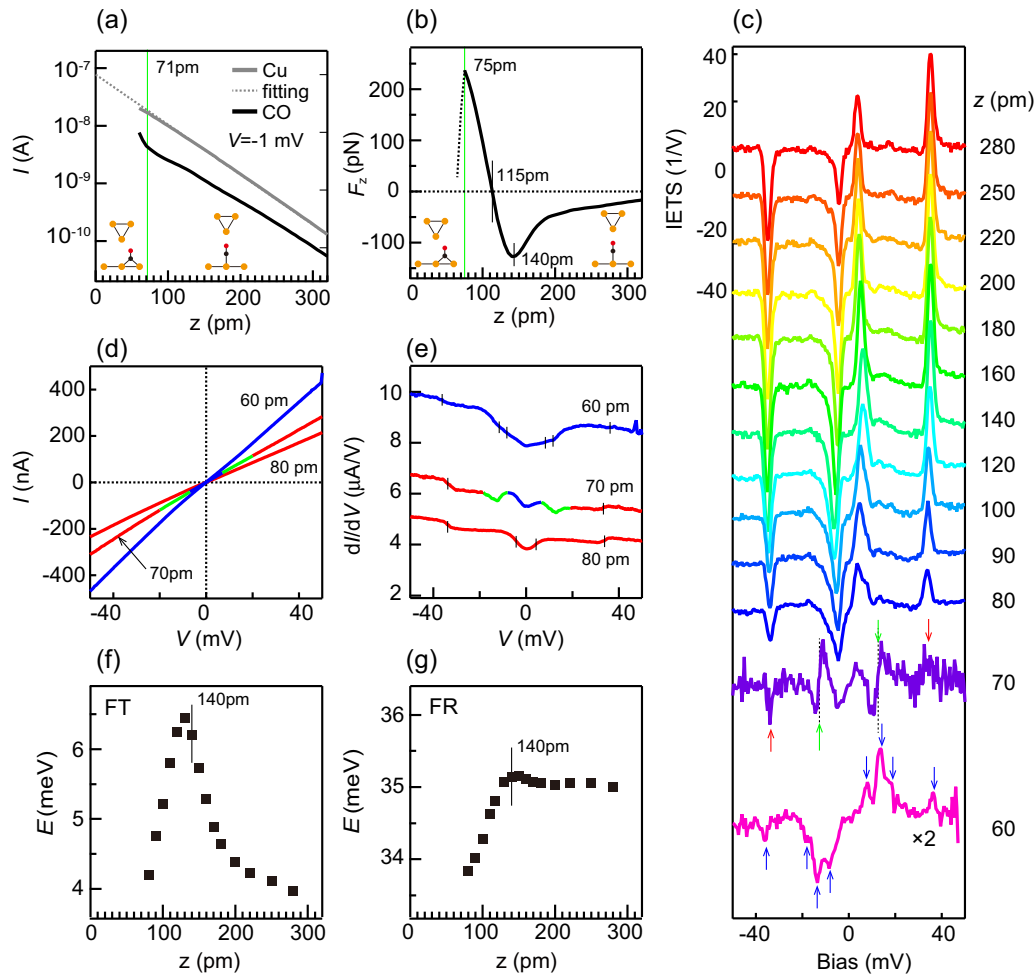


FIG. 9. Sequential processes leading to the change in the adsorption site of CO on Cu(110) from the top to the bridge site. (a) Tunneling current as a function of the tip height over a CO molecule (black) and on a Cu substrate (gray). The bias is -1 mV, and the amplitude of the sensor is 0 pm. (b) Short-range vertical force plotted as a function of tip height, where the amplitude is 20 pm, and bias is 0 mV. (c) Dataset of inelastic electron tunneling spectroscopy (IETS) dependent on the tip height for the CO molecule on the Cu(110) surface, where the tip was located on the CO molecule, and the measurement was performed in the static mode ($A = 0$ pm). Bias-dependent (d) current and (e) conductance dI/dV for CO/Cu(110) surface at three different tip heights ($z = 80, 70,$ and 60 pm), acquired simultaneously with the IETS displayed in (c). The red, blue, and green lines represent CO on top, bridge, and the transient state, respectively. Changes in the vibrational energies of the (f) frustrated translational (FT) and (g) frustrated rotational (FR) vibrational modes of CO on the top site.

Cu(110) surface at three different tip heights ($z = 80, 70,$ and 60 pm). These observations were made simultaneously with those shown in Fig. 9(c). The change in the configuration occurs at approximately these tip heights. At $z = 80$ pm, a dI/dV curve typical for CO on the top site is seen; there is a clear increase in the conductance at $\sim \pm 4$ and ± 34 mV (vertical lines). Conversely, at $z = 60$ pm, the conductance changes significantly. (1) The overall conductance becomes considerably higher than the expected value by exponential dependence on the tip height, (2) the change in conductance owing to the FR mode excitation is considerably small, and (3) the features around the FT mode excitation change significantly. At $z = 70$ pm, both the features are observed. (1) When the absolute value of the bias $|V|$ is < 7 mV (blue line), the conductance is moderately higher than that in the case of a slightly higher bias (green line). (2) When $|V|$ is > 20 mV (red line), the conductance curve is like that at $z = 80$ pm, and a change in the conductance at the FR mode

energy is seen clearly. Thus, CO conformation at $z = 70$ pm is as follows: if $|V| < 7$ mV, CO is on the bridge site; if $|V| > 20$ mV, CO is on the top site; and if $|V|$ is 7 – 20 mV (green line), the transition between the two states occurs, resulting in a structure that resembles the derivative of a Lorentzian in the IETS (represented by green arrows in Fig. 9(c) for $z = 70$ pm).

The changes in the vibrational energy shifts of CO on the top site are summarized in Fig. 9(f) for the FT mode and Fig. 9(g) for the FR mode. For the monotonically increasing attractive force regime ($z > 140$ pm), the energy of the FT mode increases monotonically, whereas that of the FR mode is almost constant, which is consistent with the results of our previous work [30]. For the less attractive and repulsive force regime ($z < 140$ pm), the vibrational energies of the FT mode decrease monotonically, and the FR mode energy begins to decrease as well, which is consistent with our DFT calculations, as discussed below. It should be noted that although the

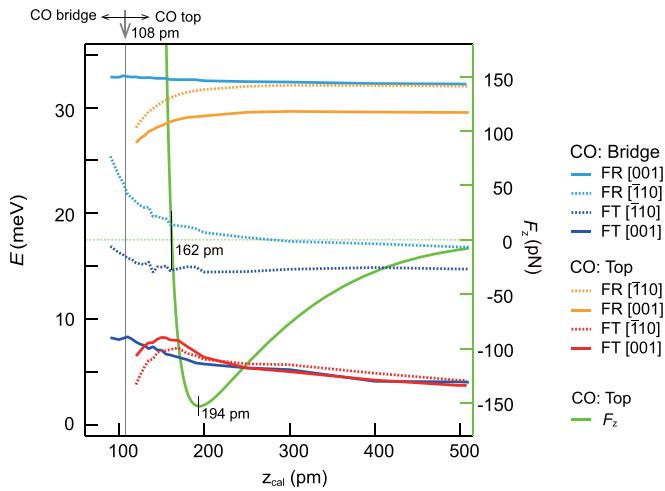


FIG. 10. Theoretical investigations of the interaction between CO-Cu(110) and a Cu_{11} tip on a top site. Energies of the frustrated translational (FT) and frustrated rotational (FR) modes of a CO molecule on a top site dependent on the tip height (z_{cal}) represented by red and orange lines, respectively. For each mode, the solid and dotted lines represent the modes along the [001] and $[\bar{1}10]$ directions, respectively. The vertical force F_z is plotted with respect to the right vertical axis (green line). The blue and light blue lines represent the FT and FR mode energies, respectively, of the CO molecule on the bridge site. Like that in the case of CO on the top site, for each mode, the solid and dotted lines represent the modes along the [001] and $[\bar{1}10]$ directions, respectively.

tendencies between the force curve and FT mode energy are similar, there are differences in the details. For example, the peak position of the attractive force is $z = 140$ pm, whereas

the peak position of the FT mode energy is $z = 130$ pm. The attractive force becomes zero at $z = 115$ pm, whereas the FT mode energy is considerably shifted (~ 6 meV) at this tip height when compared with the intrinsic energy (~ 4 meV).

The vibrational energy shifts of CO due to the interaction force from the tip were also investigated using DFT calculations. In Fig. 10, the vibrational energies of the FT (red line) and FR (orange line) modes of a CO molecule on the top site are plotted as a function of the height (z_{cal}) of the Cu_{11} tip located on the top site. For each mode, the solid and dotted lines represent the modes along the [001] and $[\bar{1}10]$ directions, respectively, where the energy difference between the two directions is small for both FT and FR modes. Indeed, in our experiment, two modes along the [001] and $[\bar{1}10]$ directions could not be discriminated for both FT and FR modes. To compare this vibrational energy shift dependence on the tip height with the interaction force, the vertical force F_z is plotted with respect to the right vertical axis (green line). For the force regime $z_{\text{cal}} > 194$ pm, the FT mode energies increase monotonically, whereas the decrease in the FR mode energies is small. When the force becomes less attractive and repulsive ($z_{\text{cal}} < 194$ pm), both FT and FR mode energies decrease significantly. These features are consistent with the experimental results shown in Figs. 9(f) and 9(g). In addition, there are further similarities in the minor points: the peak position of the attractive force is $z_{\text{cal}} = 194$ pm, which is slightly larger than the peak positions of the FT modes ($z_{\text{cal}} = 156$ – 168 pm). The attractive force becomes zero at $z_{\text{cal}} = 162$ pm; nevertheless, the FT mode energies at this tip height are still considerably shifted compared with the intrinsic energies (3.8–4.2 meV).

The blue and light blue lines in Fig. 10 represent the FT and FR mode energies, respectively, of the CO molecule on

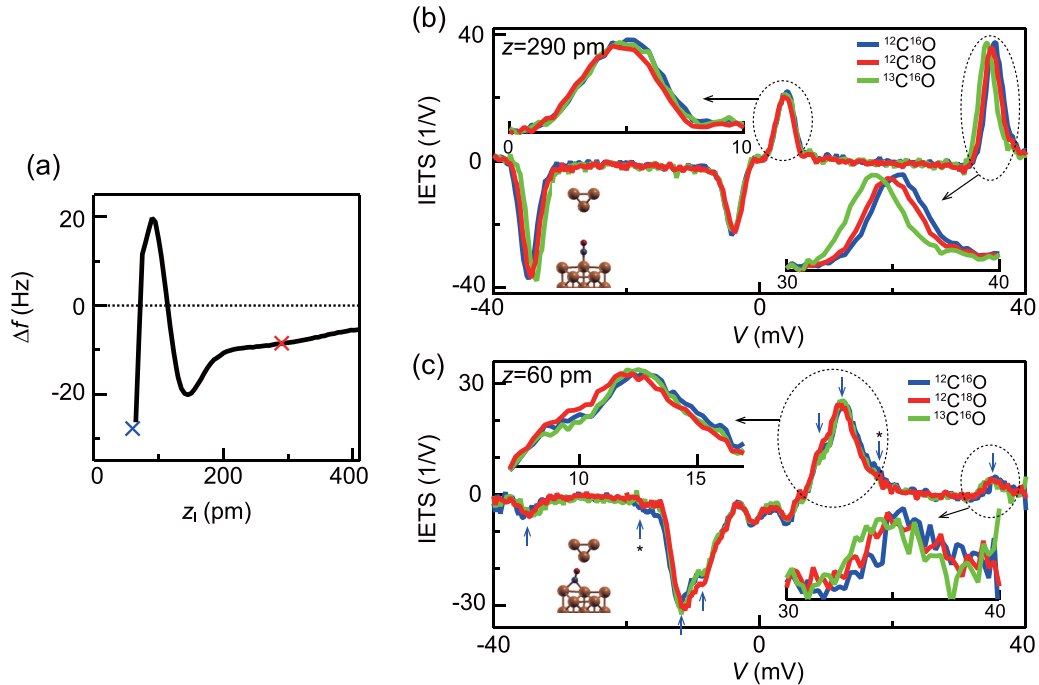


FIG. 11. Experimental isotope-dependent inelastic electron tunneling spectroscopy (IETS) for CO on top and bridge sites on Cu(110). (a) Frequency shift curve for a tip used for this measurement. IETS was measured at the two tip heights shown by the cross marks. (b) Isotope-dependent IETS for CO on a top site. The tip height was $z = 290$ pm [red cross mark in (a)]. (c) Isotope-dependent IETS for CO on a bridge site. The tip height was $z = 60$ pm [blue cross mark in (a)].

TABLE II. Experimental investigation on the low-energy vibrational energy shifts for an isotope-substituted CO molecule on Cu(110). (a) The case for CO on a top site, where the perturbation from the tip to the molecule is negligibly small ($z = 290$ pm). The numbers in the table represent the vibrational energies of CO (in parentheses, the isotope shift relative to the normal molecule). (b) Like in (a) but for CO adsorbed on a bridge site, where the vibrational energies are strongly influenced by the perturbation from the tip. The peak heights at 8 and 18 meV are so small that it is difficult to discuss the isotope dependence.

(a) CO on top site: $z = 290$ pm			
	$^{12}\text{C}^{16}\text{O}$ (meV)	$^{13}\text{C}^{16}\text{O}$ (meV)	$^{12}\text{C}^{18}\text{O}$ (meV)
FR	34.97	33.95 (−3.0%)	34.63 (−1.0%)
FT	4.02	3.99 (−0.7%)	3.79 (−5.7%)
(b) CO on bridge site: $z = 60$ pm			
	$^{12}\text{C}^{16}\text{O}$ (meV)	$^{13}\text{C}^{16}\text{O}$ (meV)	$^{12}\text{C}^{18}\text{O}$ (meV)
FR[001]	35.54	34.26 (−3.6%)	34.96 (−1.6%)
FR[$\bar{1}10$]	~18	~18	~18
FT[$\bar{1}10$]	12.33	12.13 (−1.6%)	11.68 (−5.3%)
FT[001]	~8	~8	~8

the bridge site, and their variation with the tip height is shown. Like the case of CO on the top site, for each mode, the solid and dotted lines represent the modes along the [001] and [$\bar{1}10$] directions, respectively. As discussed earlier, the most stable adsorption site changes from the top to the bridge site for a small value of z (represented by the gray arrow at $z_{\text{cal}} = 108$ pm). The energies of these four CO vibrational modes are separated from their neighboring energies at approximately this tip height, which is consistent with the experimental observations of the four peaks shown in Fig. 9(c).

Further consideration of the peak assignment of IETS for CO on the bridge site was examined using different isotopes of CO [91]. The force curve for the tip used for this measurement is shown in Fig. 11(a), where the isotope-dependent IETS was measured for the red cross point (CO on top) and blue cross point (CO on bridge). In Fig. 11(b), the isotope-dependent IETS for CO on the top site is shown. The two insets show the expanded IETS around the FT mode positive peak (left) and the FR mode positive peak (right). In the FR mode of CO on the top site, the C atom is more displaced than the O atom [30]; thus, a strong isotope shift is observed for $^{13}\text{C}^{16}\text{O}$. In the FT mode of CO, the O atom is more displaced, which results in a stronger isotope shift for $^{12}\text{C}^{18}\text{O}$ (see Table II for more details).

Figure 11(c) shows the isotope-dependent IETS for CO on a bridge site. Three clear peaks are observed at ± 8 , ± 12 , and ± 35 mV and one obscure peak at ± 18 mV. The two insets show the expanded IETS for the region of $+7$ – 17 mV (left) and $+30$ – 40 mV (right). Compared with our DFT calculations for CO on the bridge site (Fig. 10, Tables III and IV), we assign the IETS peaks observed at 8, 12, 18, and 35 mV to the FT mode along [001] and [$\bar{1}10$] and the FR mode along [$\bar{1}10$] and [001], respectively. According to our DFT calculations, the displacements of C and O in the FT and FR modes on the bridge site are like those of CO on the top site; O is displaced more in the FT modes, whereas C is displaced more

TABLE III. Theoretical investigation on the low-energy vibrational energy shifts for an isotope-substituted CO molecule on Cu(110) with the Cu_{11} tip. (a) The case of CO on a top site is shown, where the tip is located on the top site far from the surface. The numbers in the table represent the vibrational energies of CO (in parentheses, the isotope shift relative to the normal molecule). (b)–(c) Like in (a) but for the case of the tip located very close to the CO molecule, where the CO molecule on the bridge is the most stable geometry.

(a) CO on top with Cu_{11} tip: $z_{\text{cal}} = 600$ pm			
	$^{12}\text{C}^{16}\text{O}$ (meV)	$^{13}\text{C}^{16}\text{O}$ (meV)	$^{12}\text{C}^{18}\text{O}$ (meV)
FR[$\bar{1}10$]	31.937	30.919 (−3.2%)	31.611 (−1.0%)
FR[001]	29.512	28.560 (−3.2%)	29.227 (−1.0%)
FT[$\bar{1}10$]	4.160	4.129 (−0.7%)	3.962 (−4.8%)
FT[001]	3.786	3.759 (−0.7%)	3.605 (−4.8%)
(b) CO on bridge with Cu_{11} tip: $z_{\text{cal}} = 100$ pm			
	$^{12}\text{C}^{16}\text{O}$ (meV)	$^{13}\text{C}^{16}\text{O}$ (meV)	$^{12}\text{C}^{18}\text{O}$ (meV)
FR[001]	32.853	31.802 (−3.2%)	32.526 (−1.0%)
FR[$\bar{1}10$]	23.583	22.796 (−3.3%)	23.386 (−0.8%)
FT[$\bar{1}10$]	16.297	16.234 (−0.4%)	15.434 (−5.3%)
FT[001]	8.085	8.025 (−0.7%)	7.699 (−4.8%)
(c) CO on bridge with Cu_{11} tip: $z_{\text{cal}} = 90$ pm			
	$^{12}\text{C}^{16}\text{O}$ (meV)	$^{13}\text{C}^{16}\text{O}$ (meV)	$^{12}\text{C}^{18}\text{O}$ (meV)
FR[001]	32.871	31.820 (−3.2%)	32.541 (−1.0%)
FR[$\bar{1}10$]	25.385	24.487 (−3.5%)	25.236 (−0.6%)
FT[$\bar{1}10$]	16.883	16.848 (−0.2%)	15.956 (−5.5%)
FT[001]	8.254	8.192 (−0.8%)	7.860 (−4.8%)

in the FR modes. The observed significant isotope shifts by O substitution for the peak at 12 mV and by C substitution for the peak at 35 mV are consistent with these theoretical expectations (Tables III and IV).

TABLE IV. Theoretical investigation on the low-energy vibrational energy shifts for an isotope-substituted CO molecule on Cu(110) with the Cu_5 tip. (a)–(c) Like Table III but for the Cu_5 tip.

(a) CO on top with Cu_5 tip: $z_{\text{cal}} = 600$ pm			
	$^{12}\text{C}^{16}\text{O}$ (meV)	$^{13}\text{C}^{16}\text{O}$ (meV)	$^{12}\text{C}^{18}\text{O}$ (meV)
FR[$\bar{1}10$]	32.019	30.998 (−3.2%)	31.692 (−1.0%)
FR[001]	29.596	28.642 (−3.1%)	29.308 (−0.9%)
FT[$\bar{1}10$]	4.494	4.460 (−0.8%)	4.280 (−4.8%)
FT[001]	3.920	3.891 (−0.7%)	3.732 (−4.8%)
(b) CO on bridge with Cu_{11} tip: $z_{\text{cal}} = 100$ pm			
	$^{12}\text{C}^{16}\text{O}$ (meV)	$^{13}\text{C}^{16}\text{O}$ (meV)	$^{12}\text{C}^{18}\text{O}$ (meV)
FR[001]	33.154	32.140 (−3.1%)	32.762 (−1.2%)
FR[$\bar{1}10$]	21.878	21.399 (−2.2%)	21.355 (−2.4%)
FT[$\bar{1}10$]	14.942	14.742 (−1.3%)	14.326 (−4.1%)
FT[001]	10.978	10.881 (−0.9%)	10.474 (−4.6%)
(c) CO on bridge with Cu_5 tip: $z_{\text{cal}} = 90$ pm			
	$^{12}\text{C}^{16}\text{O}$ (meV)	$^{13}\text{C}^{16}\text{O}$ (meV)	$^{12}\text{C}^{18}\text{O}$ (meV)
FR[001]	32.985	31.973 (−3.1%)	32.596 (−1.2%)
FR[$\bar{1}10$]	23.945	23.167 (−3.2%)	23.711 (−1.0%)
FT[$\bar{1}10$]	16.558	16.491 (−0.4%)	15.686 (−5.3%)
FT[001]	10.517	10.424 (−0.9%)	10.034 (−4.6%)

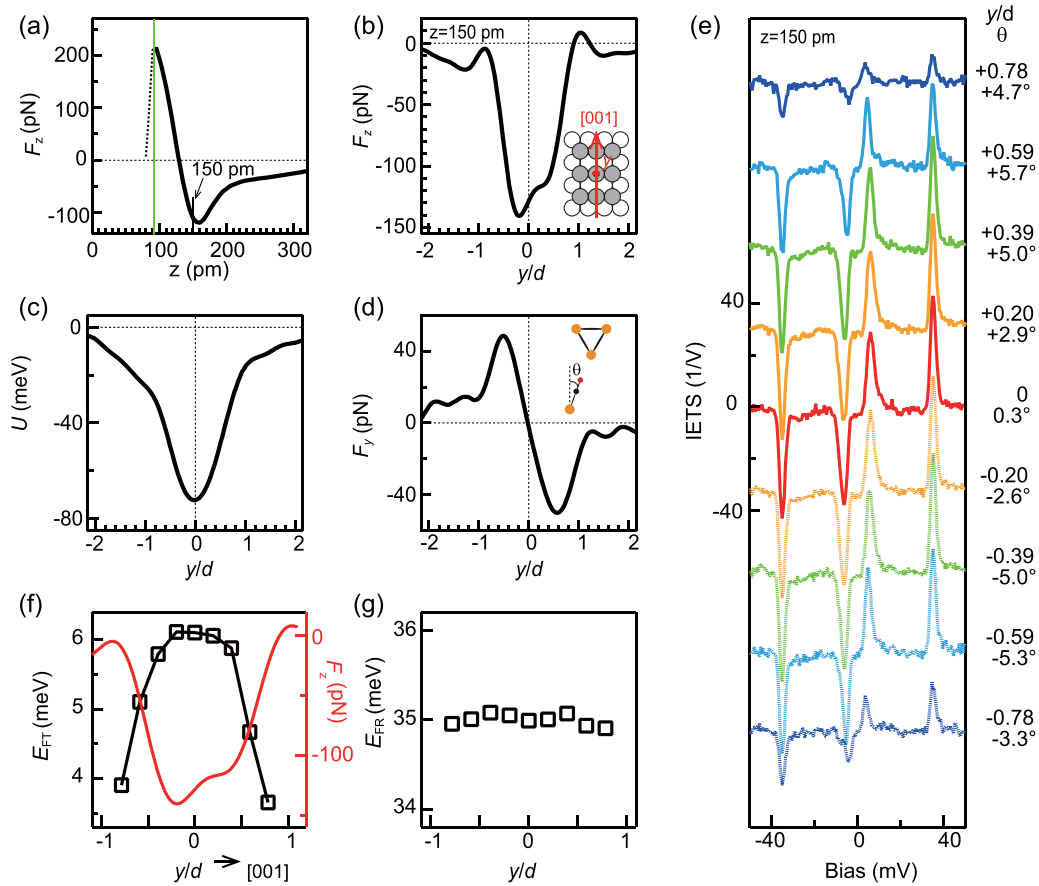


FIG. 12. Experimental inelastic electron tunneling spectroscopy (IETS) for tilted (top site) CO on Cu(110). (a) Force curve with a monoatomic tip used for this measurement. (b) Vertical force (F_z) at the tip height of $z = 150$ pm is plotted as a function of the lateral tip position (y/d). The lateral tip position changes along the [001] direction. (c) Potential energy between the CO molecule and tip at $z = 150$ pm. (d) Lateral force between the CO molecule and tip at $z = 150$ pm. (e) IETS dependent on the lateral tip position. The tip height is $z = 150$ pm. The lateral tip position y/d and CO tilt angle θ estimated using the lateral force F_y are depicted for each spectrum in the margin on the right. (f) Frustrated translational (FT) mode energy (represented by open squares) dependent on the lateral tip position plotted along with the vertical force (red curve). (g) Frustrated rotational (FR) mode energy dependent on the lateral tip position.

C. Investigation of the CO tilt process

The tilt of a CO molecule attached to a metallic tip has been reported to induce a significant change in the force curve when approaching very close to a metal surface [92]. To check whether this CO tilt induces a significant change in the vibrational states with energy dissipation, as we observed in the present case, IETS was measured by changing the lateral tip position y along the [001] direction (Fig. 12). Figure 12(a) shows the force curve with the monoatomic tip used for this measurement. Figure 12(b) shows the vertical force F_z at a tip height of $z = 150$ pm as a function of the lateral tip position, which was acquired by deconvoluting the two-dimensional frequency shift $\Delta f(y, z)$ distribution with respect to the z direction [46], where the long-range background force between the tip and Cu substrate is subtracted. Figure 12(c) shows the potential energy between the CO molecule and the tip at $z = 150$ pm, which was extracted by integrating $F_z(y, z)$ in the z direction [46]. Similarly, Fig. 12(d) shows the lateral force between the CO molecule and the tip at $z = 150$ pm, which was acquired by differentiating $U(y, z)$ along the y direction. Figure 12(e) shows the IETS at $z = 150$ pm by changing the

lateral tip position, where the normalized tip positions y/d are shown for each spectrum in the margin on the right. In addition, the CO tilt angle θ , estimated using the lateral force F_y , is shown.

In this analysis, it is assumed that the CO molecule is a single pendulum, its arm length is 251 pm, and the lateral stiffness is 2.0 N/m. In our DFT calculations, the lengths between O and C and between C and Cu were estimated to be 115 and 190 pm for top site, respectively. Thus, the distance between the Cu atom and the center of gravity of the CO molecule was 251 pm. In our experiment, the energies of the FT and FR modes for the far-tip position were ~ 4 and 35 meV, respectively. Using these vibrational energies in the classical double-pendulum mode [30], the angular force constants D_1 (for the angle between CO and CuC) and D_2 (for the angle between C and the surface normal) were estimated to be 214 and 124 zNm, respectively. Thus, the lateral spring constant of CO was estimated to be $124 \text{ zNm}/(251 \text{ pm})^2 = 2.0 \text{ N/m}$.

As shown in Fig. 12(e), each IETS curve consistently consists of two components of the FT (± 4 –6 meV) and FR (± 35 meV) modes, although a considerable CO tilt occurs. This result excludes the possibility of CO tilt for the observa-

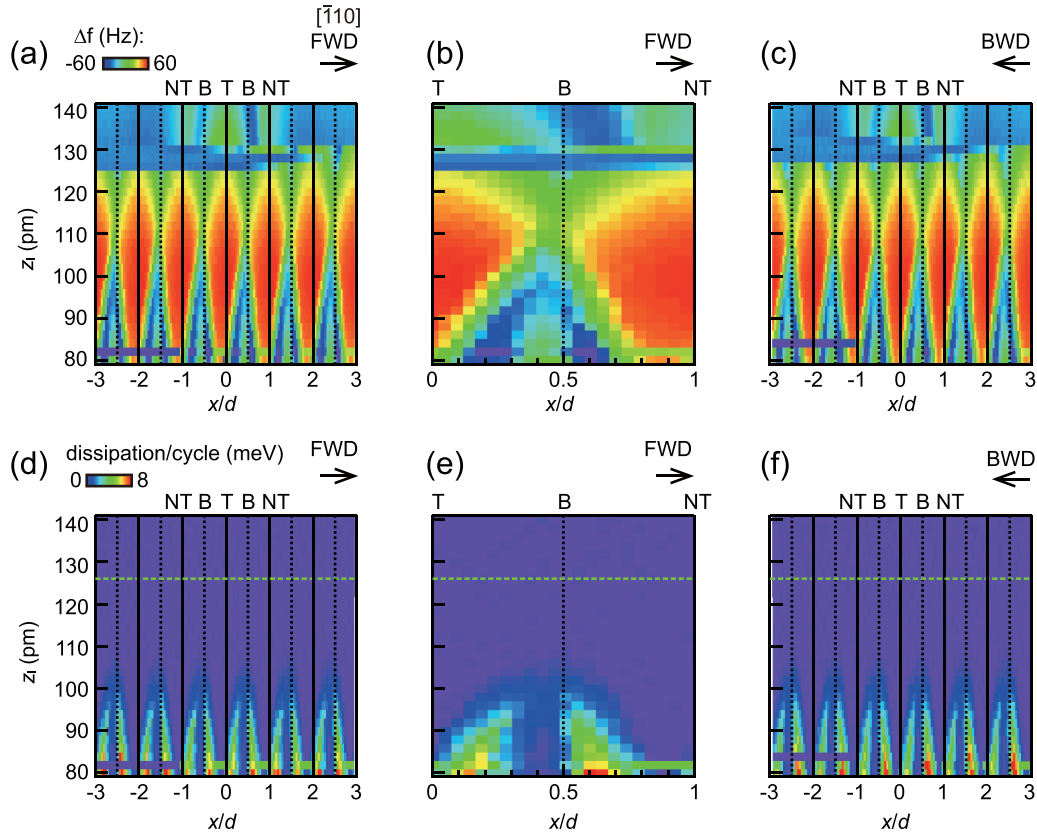


FIG. 13. Experimental energy dissipation during dragging of a CO molecule on Cu(110). (a) Frequency shift data as a function of the lateral and vertical tip positions, where the top/neighborhood top (T/NT) and bridge (B) sites are shown as solid and dotted lines, respectively. (b) An enlarged view of (a) in the range $x/d = 0$ to 1. (c) Like in (a) but for the backward scan. (d) Energy dissipation per cycle of the vertically oscillated tip, which was acquired simultaneously with (a). (e) An enlarged view of (d) in the range $x/d = 0$ to 1. (f) Like in (d) but for the case of backward scan.

tion of significantly changed IETS [$z = 60$ pm in Fig. 9(c)]. Figure 12(f) shows the FT mode energy (represented by open squares) dependent on the lateral tip position plotted along with the vertical force (red curve). A strong correlation can be observed between the FT mode energy and F_z , which is like the case in which the tip approaches vertically [Figs. 9(b) and 9(f)]. Figure 12(g) shows the FR mode energy dependence on the lateral tip position, where the FR mode energy is almost constant.

D. CO dragging with energy dissipation

The above discussion indicates that the bridge site, which is not occupied for a far tip position, is engaged at shorter tip-sample distances. This bridge site is crucial for understanding the dragging process of a CO molecule on a Cu(110) surface (Fig. 13). In this measurement, CO was initially adsorbed on the top site at $x/d = 0$, and the tip was set at $z_1 = 140$ pm and $x/d = -3$. The tip was first swept forward and then backward. After finishing one lateral scan, the tip height was decreased by 2 pm, and the lateral scan was repeated. Figure 13(a) shows the frequency shift data for the forward scan as a function of the lateral and vertical tip positions, where the top/neighborhood top (T/NT) and bridge (B) sites are shown as solid and dotted lines, respectively. Figure 13(b) shows an enlarged view of a portion of Fig. 13(a) from $x/d = 0$ to 1, and

Fig. 13(c) shows the case for the backward scan. At the initial stage of this measurement, CO stays adsorbed on the top site. Subsequently, in the backward scan at $z_1 = 132$ pm, manipulation to the neighboring top site on the right occurs. By further decreasing the tip height, the CO molecule remains at $x/d = 3$ for some time because the slightly asymmetric tip apex in this case favors manipulation to the right. Subsequently, when the tip height reaches $z_1 = 126$ pm, manipulation to the left side starts to occur, which results in the so-called dragging of the molecule, where the molecule is manipulated along the $[\bar{1}10]$ direction as if trapped by the tip. For a very small tip height ($z_1 = 82$ pm), dragging eventually fails. Figure 13(d) shows the energy dissipation per cycle of the vertically oscillated tip, which was acquired simultaneously with Fig. 13(a). An enlarged view of Fig. 13(d) within the region $x/d = 0-1$ is shown in Fig. 13(e), and the case of the backward scan is shown in Fig. 13(f). At the initial stage of dragging from $z_1 = 126$ (green dotted line) to 110 pm, CO is manipulated without a signal in the energy dissipation. However, when the tip height reaches $z_1 = 108$ pm, the onset of energy dissipation is observed for the tip over the bridge sites. By further decreasing the tip height, the peak located on the bridge sites is split into two lateral tip positions, where the dissipation energy increases.

Figure 14 shows the line scans selected from the frequency shift and dissipation measurements in Fig. 13 for both the

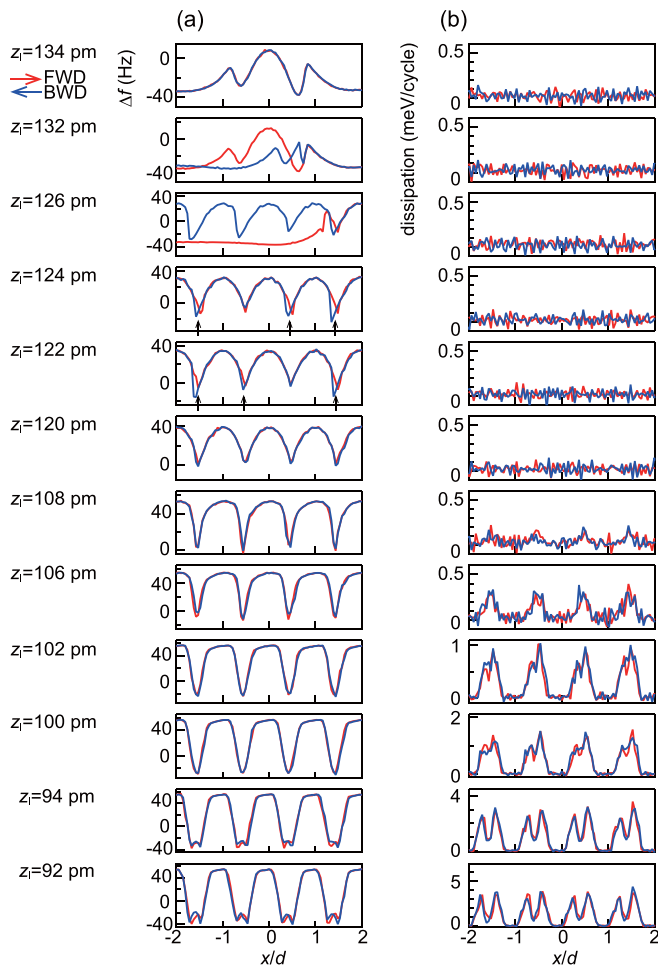


FIG. 14. Details of the experimental frequency shift and energy dissipation during CO dragging on Cu(110). (a) Selected line scans of the frequency shift measurement in Fig. 13 are shown for both the forward and backward scan directions. In Fig. 13, the scan range is from $x/d = -3$ to 3; however, only the range from $x/d = -2$ to 2 is shown here. (b) Like in (a) but for energy dissipation.

forward and backward scan directions. Notably, the line scans at $z = 124$ and 122 pm show hysteresis between the forward and backward scans around the x position, where the frequency shift shows a minimum (see black arrows).

These features of CO dragging with dissipation were also confirmed in the constant-height raster scan images (Fig. 15). In each image, the tip is initially located on the upper left corner of the image, and the CO molecule is initially adsorbed on the top site, as indicated by the cross point of the thick red lines. The fast-scan direction is horizontal, and the slow-scan direction is from top to bottom. Here, only the forward-scan direction is shown. The cross points of the vertical and lateral red lines correspond to the positions of the atoms along one atomic row. When the tip height is relatively large ($z_1 = 180$ pm), an attractive feature (decrease in Δf) appears over CO. By further approaching the tip, this attractive feature changes to a repulsive feature ($z_1 = 140$ pm), and finally, at $z_1 = 130$ pm, manipulation to the neighboring top site on the right side occurs. When z_1 decreased to 120 pm, manipulation to the left side also occurs, resulting in CO dragging. In the

initial stage of dragging, a dissipation signal is not observed. However, at $z_1 = 105$ pm, the onset of dissipation appears at the bridge sites. By lowering the tip height, the dissipation signal at the bridge sites is split into two peaks that are symmetric with respect to the bridge site.

These features of the dragging process can be interpreted using DFT calculations. Figure 16 shows the calculated potential energy between the tip and CO molecule on three adsorption sites (top, bridge, and neighboring top) by changing the lateral tip position from the top to the next top site [Fig. 16(a) for the Cu_{11} tip and Fig. 16(b) for the Cu_5 tip]. To explain the typical processes for manipulation, four cases of tip height with the Cu_{11} tip are chosen, as shown in Figs. 17(a)–17(d). In these figures, the tip that is initially on the top site at $x/d = 0.0$ is swept toward the next top site at $x/d = 1.0$, whereas the CO molecule is initially adsorbed on the top site ($x/d = 0.0$). To simplify the discussion here, we consider that a spontaneous transition occurs from the top to the bridge when their energies become identical, which implies a vanishingly small reaction barrier from top to bridge. The dotted lines are identical to the lines in Fig. 16, and the thick line represents the CO adsorption state for the forward-tip scan. Figure 17(a) shows the case in which the distance between the tip and the sample is large. As the tip moves beyond the bridge site ($x/d = 0.5$), the energy of CO on the neighboring top site (blue) is lower than that on the top site (black). However, this manipulation is not possible because of the presence of an energy barrier E_b . Figure 17(b) shows the case for the decreasing tip height, where the situation changes: at $x/d \sim 0.7$, the energies of the top and bridge sites are the same, and the manipulation to the bridge site occurs first, which results in further manipulation to the neighboring top site. Figure 17(c) shows the case for further decrease in the tip height. When the tip approaches the bridge site at $x/d = 0.5$, the energy for the bridge site (red) is already lower than that for the top site (black). In this case, the manipulation to the bridge site occurs first, and the CO molecule continues to adsorb on that location until the energy of the bridge site (red) becomes identical to that of the neighboring top site (blue). Figure 17(d) shows the case for a very low tip height, where the CO molecule on the bridge site is always stable, and no manipulation can occur.

Figure 17(e) summarizes the dragging process for the forward scan, where the onset of dragging is indicated by the dotted green line. The regions depicted by gray, light blue, and light red correspond to the CO molecule on the top, neighboring top, and bridge sites, respectively. This figure indicates that, at the initial stage of the dragging process, no dissipation signal is expected at the manipulation across the blue line because this manipulation occurs only once, even though the tip repeatedly approaches and retracts. When the tip moves deeper into the contact regime, a strong dissipation is expected for manipulation across the red line because the transition occurs repeatedly correlated with the tip oscillation. The transition across the red line initially appears over the bridge site and splits laterally into two positions as the tip height decreases. These expectations are consistent with the observations in Figs. 13–15, substantiating the microscopic picture of the manipulation steps. Like the case of the forward scan, we summarize the dragging process for the backward

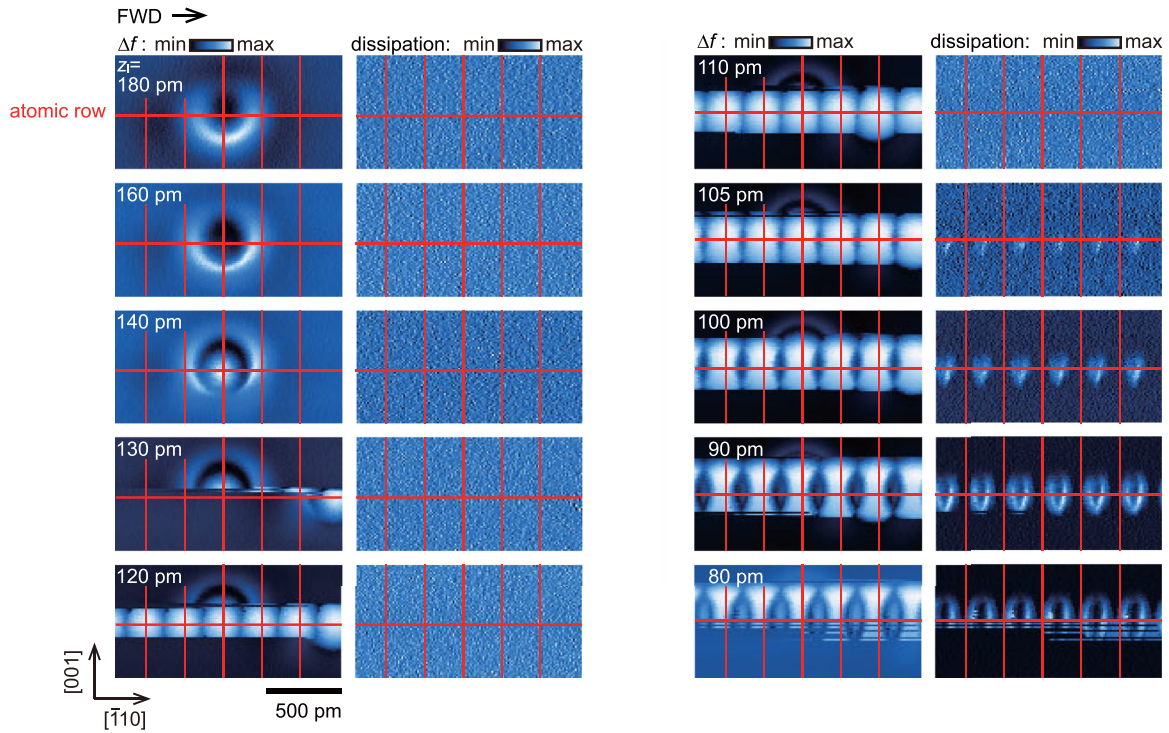


FIG. 15. Experimental frequency shift and energy dissipation images in constant height raster scans for a CO molecule on Cu(110).

scan in Fig. 17(f). The feature of this dragging process is identical to that of the forward scan; however, the slope of the blue line is opposite between the forward and backward scans. At the beginning of the dragging, the lateral tip position where the manipulation occurs is slightly different between the forward and backward scans, which becomes smaller by further decreasing the tip height. This trend is consistent with the experimentally observed asymmetries in the scan direction (Fig. 14, $z_t = 124$ and 122 pm).

Dissipation patterns like in Fig. 13 were also observed for different amplitudes ($A = 40, 60,$ and 80 pm), where its magnitude (dissipation per cycle) increases with increasing the amplitude, e.g., the peak values of dissipation per cycle at $z_t = 90$ pm are 4.0, 5.9, 7.8, and 9.9 meV for $A = 20, 40, 60,$ and 80 pm, respectively. This amplitude dependence is consistent with our discussion that the frequency of the manipulation between the top and bridge sites is generally lower than that of the oscillation owing to a small barrier for CO back to the top site from the bridge site. Moreover, this small barrier becomes smaller for a far tip position, as shown in Figs. 7 and 8 (e.g., red and orange curve in Fig. 7 for $x/d = 0.3$), indicating that, as the amplitude increases, the frequency of the manipulation becomes higher, and the dissipation per cycle as an averaged measurement becomes larger.

E. Static friction and dynamic friction

Our model of the dragging process can provide an interpretation of static and dynamic friction. Figure 18(a) shows one of the frames of the calculated energy profiles for lateral manipulation on Cu(110) from Fig. 16: Cu₁₁ tip and

$z_{\text{cal}} = 145$ pm. The black and blue lines are obtained by fitting the calculated data points with sigmoid functions, $y = b + m/[1 + \exp[(x_0 - x)/rd]]$, where $b, m, x_0,$ and r are the fitting coefficients, y is the dependent variable, and x is the independent variable. The red line is obtained by fitting it with a Gaussian function. Manipulation from the top to the neighboring top site is considered to occur when the black line intersects the red line, as shown by the green cross mark. The slope of the black line at this intersection (dotted line) corresponds to the lateral force needed to manipulate CO [46,49], i.e., static friction F_s . On the other hand, a dynamic friction force F_d can be considered a force to keep an object in motion. Considering that its origin is the sequential energy dissipation process that occurs in the motion, F_d can be estimated by dividing the energy dissipation by the periodic distance of the manipulation. In the case of Fig. 18(a), the former corresponds to the energy difference between the black and blue lines at $x/d \sim 0.7$, marked as E_d , and the latter corresponds to the distance d between the nearest-neighboring Cu atoms. Based on this idea, the static and dynamic friction can be estimated as a function of the vertical tip-sample distance, as shown in Fig. 18(b). Furthermore, the ratio of dynamic friction to static friction is plotted as a function of tip height for the two tip structures in Fig. 18(c). The ratio is 10–44%, which is consistent with the empirical law for macroscopic systems [1,3].

F. Comparison with the conventional picture of friction

The PT model [16,17] can qualitatively explain the energy dissipation process during molecular manipulation; however, only a single-hopping process is considered. As shown in Fig. 19(a), we assume the situation in which a CO molecule moves on a one-dimensional sinusoidal potential along the

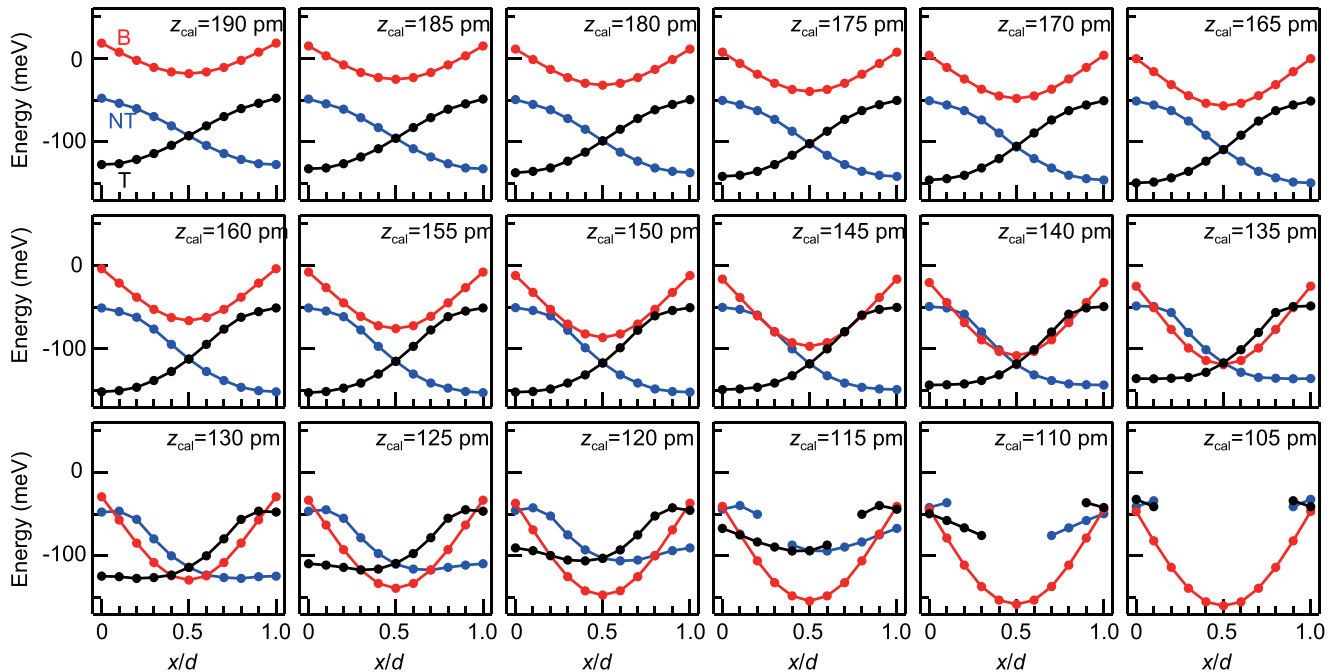
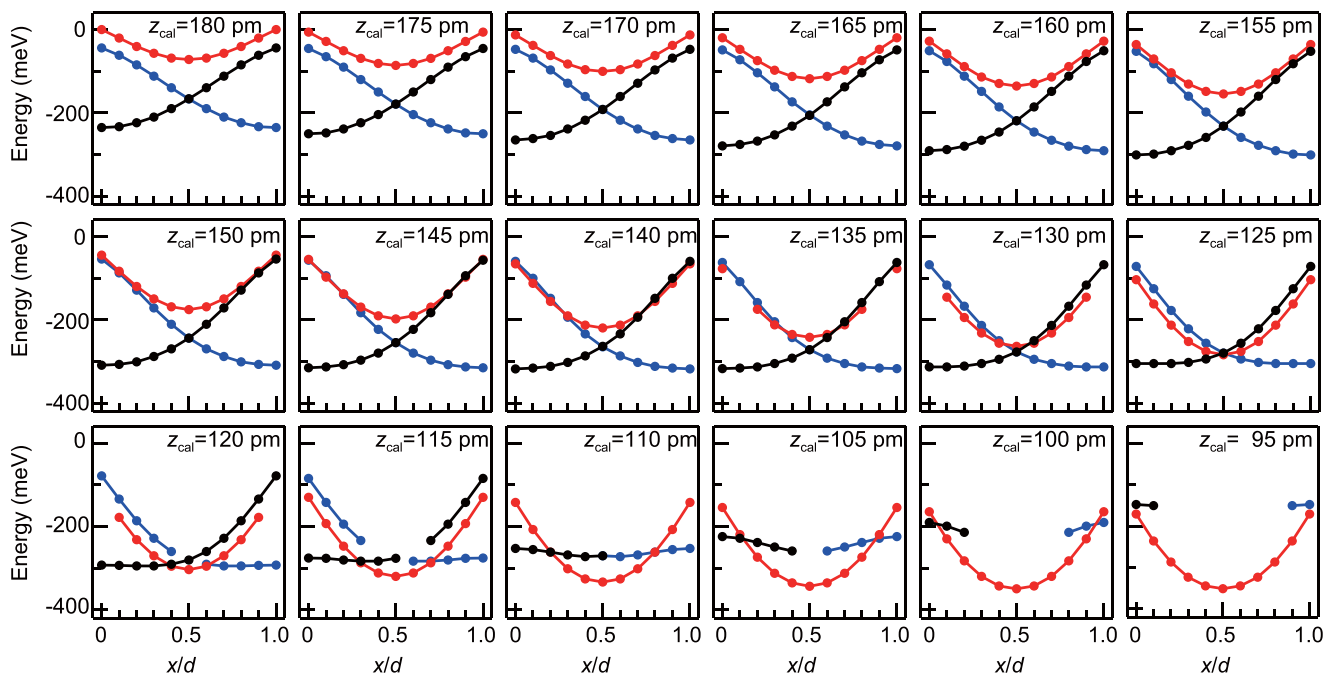
(a) Cu₁₁ Tip(b) Cu₅ Tip

FIG. 16. Calculated energy profiles for lateral CO manipulation on Cu(110). (a) Potential energies between the inert Cu₁₁ tip and CO on the three adsorption sites are plotted as a function of the lateral tip position, where the tip height is systematically changed. In each panel, the black, red, and blue lines represent CO on the top (T), bridge (B), and neighboring top (NT) site, respectively. (b) Like in (a) but for the reactive Cu₅ tip.

x axis (red line); $U_{\text{CO-Cu}} = -U_0/2 \times \cos(2\pi x_{\text{CO}}/d) + U_0/2$, where U_0 ($=97$ meV [93]) is the activation energy for manipulation, x_{CO} is the CO position, and d is the distance between the neighboring top sites. We also consider that the tip is scanned along the x axis, and the interaction between CO and the tip can be expressed by a Gaussian (blue line) as follows: $U_{\text{CO-tip}} = -E_0 \times \exp\{-[(x_{\text{CO}} - x_{\text{tip}})/wd]^2\}$, where E_0 is the

maximum attractive interaction potential, x_{tip} is the tip position, and w is the width of the potential temporarily adopted to be 0.8 from our DFT calculations.

Subsequently, the total potential energy $U_{\text{tot}} = U_{\text{CO-Cu}} + U_{\text{CO-tip}}$ for the case $E_0 = 3U_0$ is plotted as a function of x_{CO} and x_{tip} in Fig. 19(b). The dashed line corresponds to the minimum energy for the tip moving from the initial top site

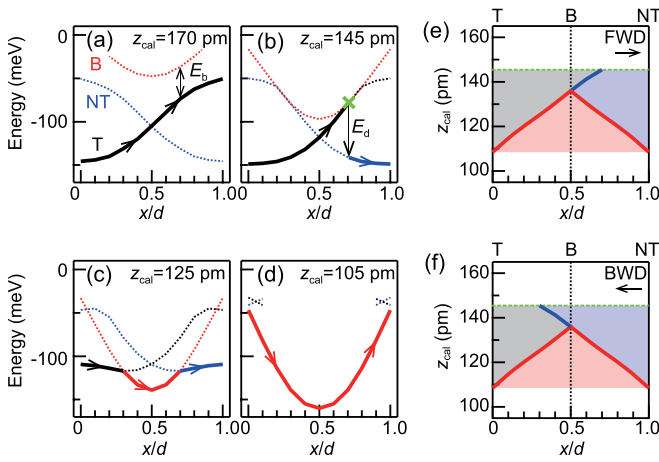


FIG. 17. Theoretical investigation of the CO dragging process on Cu(110) with the Cu₁₁ tip. (a)–(d) The potential energies between the tip and CO adsorbed on the top (black), bridge (red), and neighboring top (blue) sites are plotted as a function of the lateral tip position for four selected tip heights. (e) The dragging process for the forward scan is summarized. (f) Like in (e) but for the case of backward scan.

($x_{\text{tip}}/d = 0$) to the neighboring top site ($x_{\text{tip}}/d = 1$). The solid line represents the actual trajectory of the CO molecule for the tip scan at 0 K. The cross-sections of the potential U_{tot} for the three tip positions $x_{\text{tip}}/d = 0$ (red), 0.55 (green), and 0.8 (blue) are shown in Fig. 19(c). When the tip is located on the initial top site ($x_{\text{tip}}/d = 0$), the top site is most stable for CO. When the tip is located beyond the bridge site ($x_{\text{tip}}/d = 0.55$), the most stable site is changed to the neighboring top site. However, manipulation does not occur at 0 K, as an energy barrier of ~ 15 meV in the green line (2) would still need to be overcome. When the tip moves further toward the neighboring top site ($x_{\text{tip}}/d = 0.8$), as shown by the blue line (3), the barrier disappears resulting in CO manipulation, where energy dissipation can be expected.

This model clearly illustrates the crucial process of friction, that is, the stick-slip motion. However, to correctly understand the process occurring in the actual system, DFT calculations are mandatory because the actual potentials between CO, Cu surface, and tip are more complicated than the simple sinusoidal for $U_{\text{CO-Cu}}$ and the Gaussian for $U_{\text{CO-tip}}$ (Figs. 7, 8, and 16). For example, if we do not consider the additional adsorption site at the bridge site, as explained, we cannot interpret the precise shape of the energy dissipation observed in the experiment.

The situation is the same even for adopting the repulsive potential [Fig. 19(d)], as in the experiment, in the PT model. The stick-slip motion of a CO molecule pushed forward is expected, before the tip reaches the CO position, as shown in Fig. 19(e) and 19(f), but again, DFT calculations are mandatory to interpret the additional adsorption site at the bridge site, and the experimental observation that the CO molecule is manipulated beyond the tip position, although the interaction force is repulsive.

G. Comparison with the Cu(111) surface

The occurrence of the intermediate state in the manipulation can be observed in another surface. Figure 20(a) shows the constant-height frequency shift image of a CO molecule dragged on a Cu(111) surface by a metallic tip, and Fig. 20(b) shows the simultaneously observed dissipation image. The fast-scan direction was lateral ($[\bar{1}10]$), and the slow-scan direction was vertical. The tip height was set at the point at which the dissipation signal began to appear. Figures 20(c) and 20(d) show the cross-sections of the dissipation image along line x_1 that passes through the top sites and line x_2 that passes through the hollow sites, respectively. In Figs. 20(c) and 20(d), strong dissipation signals are observed at the bridge and hollow sites, respectively.

These features of the dissipation signals were investigated using DFT calculations, where the contributions from the intermediate states were considered. As shown in Figs. 21(a) and 21(b), two cases of the tip-scan along the $[\bar{1}10]$ direction were investigated: line x_1 that passes through the top sites and

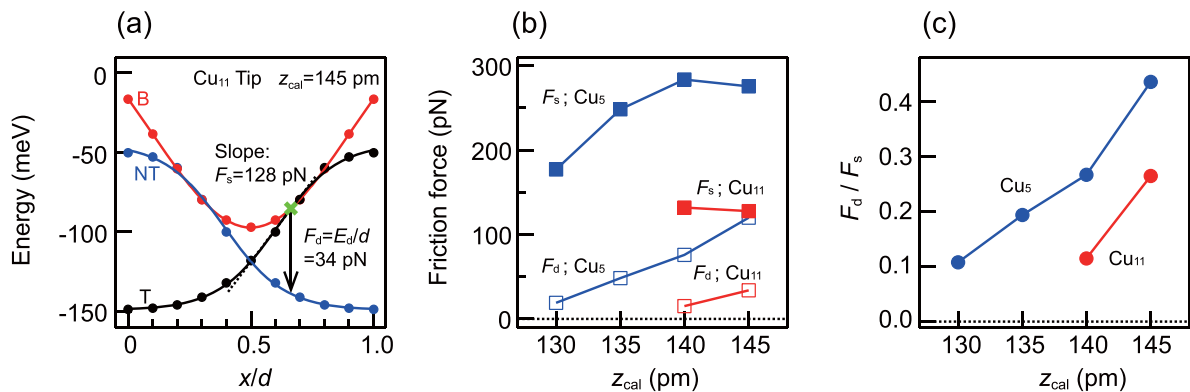


FIG. 18. Theoretical description of static friction and dynamic friction. (a) One of the frames of the calculated energy profiles for lateral manipulation on Cu(110) from Fig. 16: Cu₁₁ tip and $z_{\text{cal}} = 145$ pm. (b) Static and dynamic friction as a function of tip height. (c) The ratio of dynamic friction to static friction is plotted as a function of tip height. Note that the method for estimating the static and dynamic friction can be applied to cases corresponding to Fig. 17(b). For even lower tip heights, as in the case of Fig. 17(c), it is in principle possible to estimate the static friction and dynamic friction theoretically. However, additional nudged elastic band (NEB) calculations would be required.

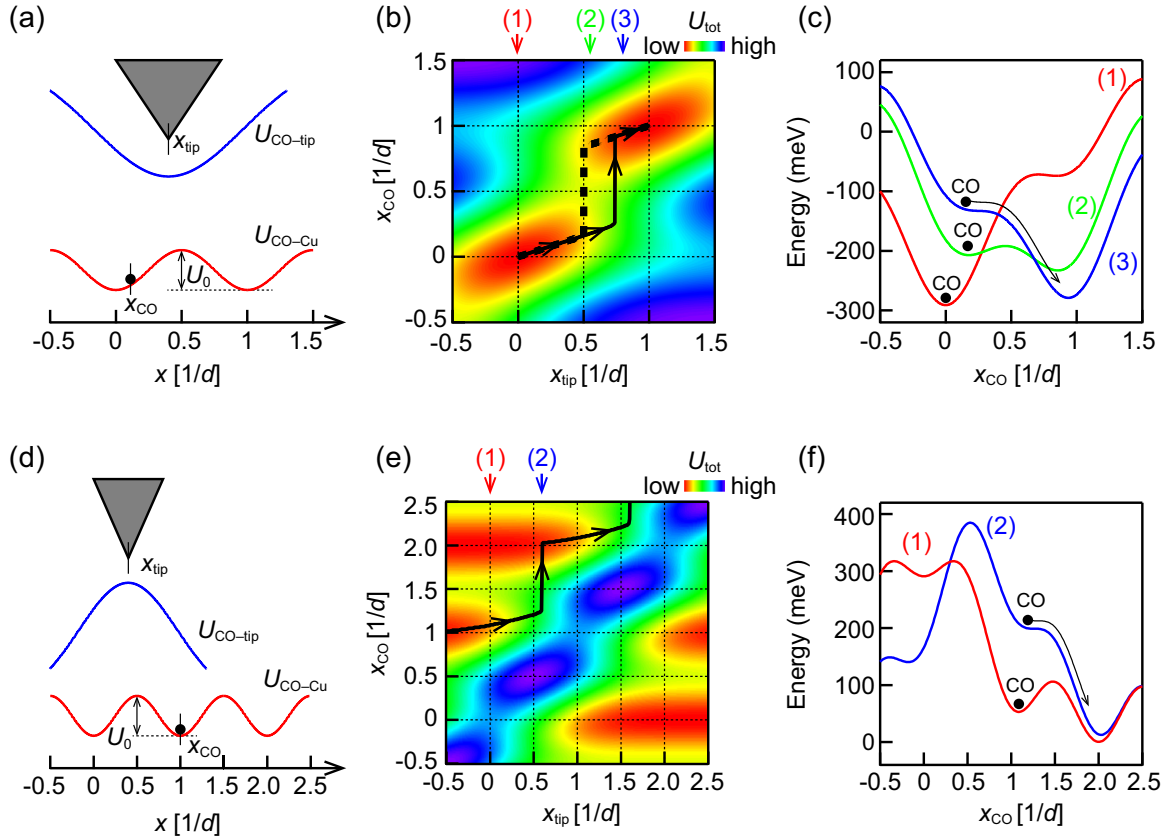


FIG. 19. The Prandtl–Tomlinson (PT) model to qualitatively explain the energy dissipation process during manipulation, where only a single hopping process is considered. (a) Schematic picture of the situation where a CO molecule moves on a one-dimensional sinusoidal potential along the x axis (red line) under the attractive potential from the tip. (b) The total potential energy $U_{\text{tot}} = U_{\text{CO-Cu}} + U_{\text{CO-tip}}$ for the case of $E_0 = 3U_0$ is plotted as a function of x_{CO} and x_{tip} . (c) U_{tot} for the three tip positions: $x_{\text{tip}}/d = 0$ (red), 0.55 (green), and 0.8 (blue). (d) The same as (a) but for the case where the potential from the tip is repulsive. (e) The total potential energy for the case of $E_0 = -3U_0$ is plotted as a function of x_{CO} and x_{tip} . The CO molecule is initially located at $x_{\text{CO}}/d = 1$. (f) U_{tot} for the two tip positions: $x_{\text{tip}}/d = 0$ (red) and 0.6 (blue), indicating that the CO molecule is manipulated from the top site ($x_{\text{CO}}/d = 1$) to the neighboring top site ($x_{\text{CO}}/d = 2$) when the tip reaches $x_{\text{tip}}/d = 0.6$: the CO molecule is pushed forward before the tip reaches the position of the CO molecule ($x_{\text{CO}}/d = 1$).

line x_2 that passes through the hexagonal close-packed (hcp) hollow sites.

In Fig. 21(c), the calculated potential energies of a CO molecule with the Cu_{11} tip are shown, where the tip is swept along the line x_1 at a constant height ($z_{\text{cal}} = 160$ pm). In this figure, the tip initially located on the top site ($x_1/d = 0$) is swept toward the neighboring top site at $x_1/d = 1.0$. The black, red, and blue dotted lines represent the cases of CO adsorption on the top (T), bridge (B), and neighboring top (NT) sites, respectively. The thick line represents the actual CO adsorption sites during the lateral tip scan. Manipulation of the CO molecule from the top to the bridge or from the bridge to the neighboring top occur when the tip is located around the bridge site. These manipulations should accompany the energy dissipation when the tip oscillates vertically, which is consistent with the observations in Figs. 20(b) and 20(c).

In Fig. 21(d), the tip initially located on the hcp hollow site ($x_2/d = 0$) is swept toward the neighboring hcp hollow site at $x_2/d = 1.0$. In this case, we considered the following CO adsorption sites: hcp hollow (H; in golden yellow), neighboring hcp hollow (NH; in light blue), two bridges (B1; in red, B2; in orange), top (T; in black), and face-centered cubic

hollow (F; in green) sites. The thick line represents the actual CO adsorption sites during the lateral tip scan. Manipulation of the CO molecule from the hollow to the top via bridge (B1) occurs when the tip is located around the initial hollow site. Similarly, manipulation from the top to the neighboring hollow via a bridge (B2) occurs when the tip is located around the neighboring hollow site. These manipulations should accompany the energy dissipation for the vertical tip oscillation, which is consistent with the observations shown in Figs. 20(b) and 20(d).

Finally, Figs. 21(e) and 21(f) show the case for the Cu_5 tip, where the other parameters are identical to those in Figs. 21(c) and 21(d). In this case, no energy dissipation is expected for this tip height ($z_{\text{cal}} = 160$ pm). However, by lowering the tip height, situations like those in Figs. 21(c) and 21(d) are expected.

IV. CONCLUSIONS

We investigated the interaction between CO on a Cu surface and a metallic tip using noncontact AFM, STM-IETS, and DFT calculations and found the following [74]: (1) When

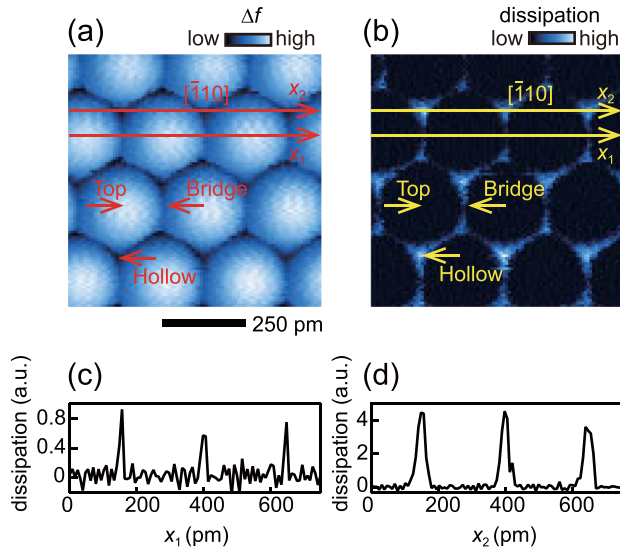


FIG. 20. Experimental energy dissipation of a CO molecule dragged on the Cu(111) surface. Constant-height (a) frequency shift and (b) dissipation image of CO dragged by a metallic tip. This dissipation image is like the case of dragging a Co atom on a Pt(111) surface [46], although its mechanism was unclear. Cross-sections of the dissipation image along the (c) line x_1 that passes through the top sites and (d) line x_2 that passes through the hollow sites.

the tip approaches CO on the Cu(110) surface around the top site, the stable adsorption site switches from the top to the bridge site. (2) When the tip oscillates, the switching of the adsorption sites with energy dissipation occurs correlated with the tip oscillation. (3) When the tip position is close to the neighboring top site, manipulation from the top to the neighboring top site occurs through the bridge site. (4) Even when the tip oscillates, such manipulation occurs only once, thereby the dissipation signal is not observed as a time average. Furthermore, (5) such a bridge site plays a crucial role as an intermediate state in the CO-dragging process. (6) The concept of static and dynamic friction in molecular manipulation can be clearly distinguished. (7) The role of intermediate states is also important for Cu(111) substrates.

A future prospect of this work [74] is the actual measurement of dynamic frictional force, which can be achieved by oscillating the probe tip laterally [20,26]. It is also important to measure the dynamic frictional forces at different temperatures. At higher temperatures, manipulation with the help of thermal energy is possible, which would reduce the dynamic frictional force. Conversely, higher temperatures will also cause thermal diffusion in unintended directions owing to thermal energy. The contribution of these processes determines the conditions for the lowest dynamic friction in molecular manipulation. The greatest advantage in this paper is that we provide an unambiguous understanding of the phenomenon, which can be used to develop a study that includes energy dissipation pathways, such as the creation of electron-hole pairs and substrate phonons [1,4]. Regarding the importance of intermediate states in the manipulation path, we found that they are valid regardless of the orientation of the Cu substrate, but further generality of the mechanism is desirable. In pre-

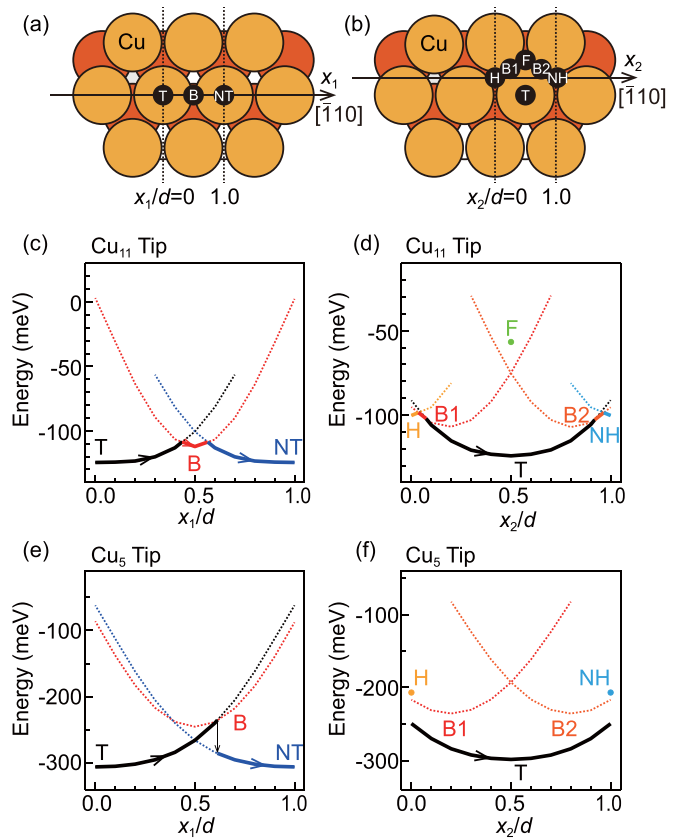


FIG. 21. Theoretical investigation of the CO dragging process with energy dissipation of a CO molecule on Cu(111). Two cases of the tip scan along the $[\bar{1}10]$ direction: (a) line x_1 that passes through the top sites and (d) line x_2 that passes through the hcp hollow sites. Calculated potential energies of a CO molecule at various adsorption sites with the Cu_{11} tip, where the tip is swept along the (c) line x_1 and (d) line x_2 at a constant height ($z_{\text{cal}} = 160$ pm). (e) and (f) Like in (c) and (d) but for the case of the Cu_5 tip.

vious manipulation studies dealing with atoms and larger molecules, such as perylenetetracarboxylic dianhydride, similar energy dissipation was reported [46,48], and we expect the contribution of intermediate states to be important in these systems as well.

Herein, we showed that the change in the vibrational energy when the probe tip is brought close to the molecule is in good agreement between the experimental and theoretical results. Previously [30], some of us discussed this change in vibrational energy from two points of view: (1) the force from the tip and (2) the conformational change of the molecule subjected to the force. In the future, it will be necessary to extend the previous discussion, analyze the change in the bond lengths and tilt angle based on charge transfer [68], and relate them to the changes in vibrational energy. The separation of chemical bonding forces from vdW forces is also important [64]. We expect that these future analyses of CO-tip interaction based on DFT calculations would contribute to the precise interpretation of high-resolution imaging with a CO-functionalized tip, for example, the images with an atomically sized cantilever without an external oscillation [60,61,63] and the repulsive ring surrounding an attractive dip when

imaging an adatom [27,64] (like the images shown in Fig. 15, $z_1 = 180\text{--}160$ pm).

We investigated the details of manipulation by force from the probe tip [74]; however, it is also important to relate manipulation via vibrational excitation by tunneling currents [66–69]. As revealed in this paper, the potential energy surface in manipulation changes significantly when the tip position is changed. Thus, an analysis that considers the tip-induced change in the potential energy surface is necessary to solve the open question [68] of the substrate dependence of CO manipulation through vibrational excitations. The control of the potential energy surface by the tip is also important when chemical reactions, such as rotation and isomerization, are induced on the surface [70–73]. The advantage of the method presented in this paper is that the dissipation energy can be measured simultaneously with the interaction potential, which is expected to be applied to synthetic reactions on surfaces such as catalysts.

The simulation input/output dataset is freely available [84].

ACKNOWLEDGMENTS

The authors thank Robert W. Carpick, Enrico Gnecco, Ferdinand Huber, Takashi Kumagai, Sonia Matencio, Daniel Meuer, Masao Obata, Hiroshi Okuyama, Magnus Paulsson, Angelo Peronio, Bo Persson, Jascha Repp, Akitoshi Shiotari, Toshiki Sugimoto, and Jay Weymouth for their valuable inputs into this research. This paper was partially supported by funding from Deutsche Forschungsgemeinschaft (Project No. CRC 1277, Project A02), by JSPS KAKENHI Grants No. 16K04959, No. 16KK0096, and No. 20K05320, the European Union's Horizon 2020 program (Grant No. 863098), and by Spanish MCIN/AEI/10.13039/501100011033 Grant No. PID2020-115406GB-I00. N.O. appreciates University of Regensburg for the opportunity to conduct this study as a visiting professor.

-
- [1] B. N. J. Persson, *Sliding Friction: Physical Principles and Applications* (Springer-Verlag, Berlin, 2000).
- [2] A. M. Wodtke, J. C. Tully, and D. J. Auerbach, Electronically non-adiabatic interactions of molecules at metal surfaces: Can we trust the Born–Oppenheimer approximation for surface chemistry? *Int. Rev. Phys. Chem.* **23**, 513 (2004).
- [3] A. Vanossi, N. Manini, M. Urbakh, S. Zapperi, and E. Tosatti, Colloquium: Modeling friction: From nanoscale to mesoscale, *Rev. Mod. Phys.* **85**, 529 (2013).
- [4] J. Y. Park and M. Salmeron, Fundamental aspects of energy dissipation in friction, *Chem. Rev.* **114**, 677 (2014).
- [5] R. Pawlak, S. Kawai, T. Meier, T. Glatzel, A. Baratoff, and E. Meyer, Single-molecule manipulation experiments to explore friction and adhesion, *J Phys D Appl Phys* **50**, 113003 (2017).
- [6] T. Takaoka and T. Komeda, Estimation of friction of a single chemisorbed molecule on a surface using incident atoms, *Phys. Rev. Lett.* **100**, 046104 (2008).
- [7] O. Bunermann, H. Y. Jiang, Y. Dorenkamp, A. Kandratsenka, S. M. Janke, D. J. Auerbach, and A. M. Wodtke, Electron-hole pair excitation determines the mechanism of hydrogen atom adsorption, *Science* **350**, 1346 (2015).
- [8] F. Hofmann and J. P. Toennies, High-resolution helium atom time-of-flight spectroscopy of low-frequency vibrations of adsorbates, *Chem. Rev.* **96**, 1307 (1996).
- [9] B. N. J. Persson and M. Persson, Damping of vibrations in molecules adsorbed on a metal-surface, *Surf. Sci.* **97**, 609 (1980).
- [10] J. C. Tully, M. Gomez, and M. Head-Gordon, Electronic and phonon mechanisms of vibrational-relaxation—CO on Cu(100), *J. Vac. Sci. Technol. A* **11**, 1914 (1993).
- [11] L. Gross, Recent advances in submolecular resolution with scanning probe microscopy, *Nature Chem.* **3**, 273 (2011).
- [12] K. Bian, C. Gerber, A. J. Heinrich, D. J. Müller, S. Scheuring, and J. Ying, Scanning probe microscopy, *Nat. Rev. Methods Primers* **1**, 36 (2021).
- [13] C. M. Mate, G. M. McClelland, R. Erlandsson, and S. Chiang, Atomic-Scale Friction of a Tungsten Tip on a Graphite Surface, *Phys. Rev. Lett.* **59**, 1942 (1987).
- [14] E. Gnecco, R. Bennewitz, T. Gyalog, C. Loppacher, M. Bammerlin, E. Meyer, and H. J. Guntherodt, Velocity Dependence of Atomic Friction, *Phys. Rev. Lett.* **84**, 1172 (2000).
- [15] Q. Li, T. E. Tullis, D. Goldsby, and R. W. Carpick, Frictional ageing from interfacial bonding and the origins of rate and state friction, *Nature (London)* **480**, 233 (2011).
- [16] L. Prandtl, Ein Gedankenmodell zur kinetischen Theorie der festen Körper, *Z. angew. Math. Mech.* **8**, 85 (1928).
- [17] G. A. Tomlinson, A molecular theory of friction, *Philos. Mag. J. Sci.* **7**, 905 (1929).
- [18] N. Sasaki and M. Tsukada, Effect of microscopic nonconservative process on noncontact atomic force microscopy, *Jpn. J. Appl. Phys.* **39**, L1334 (2000).
- [19] F. J. Giessibl, The qPlus sensor, a powerful core for the atomic force microscope, *Rev. Sci. Instrum.* **90**, 011101 (2019).
- [20] F. J. Giessibl, M. Herz, and J. Mannhart, Friction traced to the single atom, *Proc. Natl. Acad. Sci. USA* **99**, 12006 (2002).
- [21] N. Oyabu, P. Pou, Y. Sugimoto, P. Jelinek, M. Abe, S. Morita, R. Perez, and O. Custance, Single Atomic Contact Adhesion and Dissipation in Dynamic Force Microscopy, *Phys. Rev. Lett.* **96**, 106101 (2006).
- [22] T. Arai, R. Inamura, D. Kura, and M. Tomitori, Energy dissipation unveils atomic displacement in the noncontact atomic force microscopy imaging of Si(111)-(7 × 7), *Phys. Rev. B* **97**, 115428 (2018).
- [23] L. N. Kantorovich and T. Trevethan, General Theory of Microscopic Dynamical Response in Surface Probe Microscopy: From Imaging to Dissipation, *Phys. Rev. Lett.* **93**, 236102 (2004).
- [24] S. Kawai, A. Benassi, E. Gnecco, H. Sode, R. Pawlak, X. L. Feng, K. Mullen, D. Passerone, C. A. Pignedoli, P. Ruffieux *et al.*, Superlubricity of graphene nanoribbons on gold surfaces, *Science* **351**, 957 (2016).

- [25] R. Pawlak, W. G. Ouyang, A. E. Filippov, L. Kalikhman-Razvozzov, S. Kawai, T. Glatzel, E. Gnecco, A. Baratoff, Q. S. Zheng, O. Hod *et al.*, Single-molecule tribology: Force microscopy manipulation of a porphyrin derivative on a copper surface, *ACS Nano* **10**, 713 (2016).
- [26] A. J. Weymouth, E. Riegel, O. Gretz, and F. J. Giessibl, Strumming a Single Chemical Bond, *Phys. Rev. Lett.* **124**, 196101 (2020).
- [27] M. Emmrich, F. Huber, F. Pielmeier, J. Welker, T. Hofmann, M. Schneiderbauer, D. Meuer, S. Polesya, S. Mankovsky, D. Kodderitzsch *et al.*, Subatomic resolution force microscopy reveals internal structure and adsorption sites of small iron clusters, *Science* **348**, 308 (2015).
- [28] B. C. Stipe, M. A. Rezaei, and W. Ho, Single-molecule vibrational spectroscopy and microscopy, *Science* **280**, 1732 (1998).
- [29] L. Vitali, R. Ohmann, K. Kern, A. Garcia-Lekue, T. Frederiksen, D. Sanchez-Portal, and A. Arnau, Surveying molecular vibrations during the formation of metal-molecule nanocontacts, *Nano Lett.* **10**, 657 (2010).
- [30] N. Okabayashi, A. Peronio, M. Paulsson, T. Arai, and F. J. Giessibl, Vibrations of a molecule in an external force field, *Proc. Natl. Acad. Sci. USA* **115**, 4571 (2018).
- [31] B. Q. Luan and M. O. Robbins, The breakdown of continuum models for mechanical contacts, *Nature (London)* **435**, 929 (2005).
- [32] Y. F. Mo, K. T. Turner, and I. Szlufarska, Friction laws at the nanoscale, *Nature (London)* **457**, 1116 (2009).
- [33] J. T. Yates, Chemisorption on surfaces—An historical look at a representative adsorbate - carbon-monoxide, *Surf. Sci.* **299**, 731 (1994).
- [34] P. J. Feibelman, B. Hammer, J. K. Norskov, F. Wagner, M. Scheffler, R. Stumpf, R. Watwe, and J. Dumesic, The CO/Pt(111) puzzle, *J. Phys. Chem. B* **105**, 4018 (2001).
- [35] M. Gajdoš, A. Eichler, and J. Hafner, CO adsorption on close-packed transition and noble metal surfaces: Trends from ab initio calculations, *J. Phys.: Condens. Matter* **16**, 1141 (2004).
- [36] Q. M. Hu, K. Reuter, and M. Scheffler, Towards an Exact Treatment of Exchange and Correlation in Materials: Application to the “CO Adsorption Puzzle” and other Systems, *Phys. Rev. Lett.* **98**, 176103 (2007).
- [37] M. Dion, H. Rydberg, E. Schroder, D. C. Langreth, and B. I. Lundqvist, Van der Waals Density Functional for General Geometries, *Phys. Rev. Lett.* **92**, 246401 (2004).
- [38] G. Roman-Perez and J. M. Soler, Efficient Implementation of a van der Waals Density Functional: Application to Double-Wall Carbon Nanotubes, *Phys. Rev. Lett.* **103**, 096102 (2009).
- [39] J. Klimeš, D. R. Bowler, and A. Michaelides, Chemical accuracy for the van der Waals density functional, *J. Phys.: Condens. Matter* **22**, 022201 (2010).
- [40] K. Lee, E. D. Murray, L. Kong, B. I. Lundqvist, and D. C. Langreth, Higher-accuracy van der Waals density functional, *Phys. Rev. B* **82**, 081101(R) (2010).
- [41] P. Lazić, M. Alaei, N. Atodiresei, V. Caciuc, R. Brako, and S. Blügel, Density functional theory with nonlocal correlation: A key to the solution of the CO adsorption puzzle, *Phys. Rev. B* **81**, 045401 (2010).
- [42] D. M. Eigler and E. K. Schweizer, Positioning single atoms with a scanning tunneling microscope, *Nature (London)* **344**, 524 (1990).
- [43] L. Bartels, G. Meyer, and K. H. Rieder, Basic Steps of Lateral Manipulation of Single Atoms and Diatomic Clusters with a Scanning Tunneling Microscope Tip, *Phys. Rev. Lett.* **79**, 697 (1997).
- [44] A. Kuhnle, G. Meyer, S. W. Hla, and K. H. Rieder, Understanding atom movement during lateral manipulation with the STM tip using a simple simulation method, *Surf. Sci.* **499**, 15 (2002).
- [45] J. A. Stroscio and R. J. Celotta, Controlling the dynamics of a single atom in lateral atom manipulation, *Science* **306**, 242 (2004).
- [46] M. Ternes, C. P. Lutz, C. F. Hirjibehedin, F. J. Giessibl, and A. J. Heinrich, The force needed to move an atom on a surface, *Science* **319**, 1066 (2008).
- [47] B. Wolter, Y. Yoshida, A. Kubetzka, S. W. Hla, K. von Bergmann, and R. Wiesendanger, Spin Friction Observed on the Atomic Scale, *Phys. Rev. Lett.* **109**, 116102 (2012).
- [48] G. Langewisch, J. Falter, H. Fuchs, and A. Schirmeisen, Forces During the Controlled Displacement of Organic Molecules, *Phys. Rev. Lett.* **110**, 036101 (2013).
- [49] M. Emmrich, M. Schneiderbauer, F. Huber, A. J. Weymouth, N. Okabayashi, and F. J. Giessibl, Force Field Analysis Suggests a Lowering of Diffusion Barriers in Atomic Manipulation Due to Presence of STM Tip, *Phys. Rev. Lett.* **114**, 146101 (2015).
- [50] J. Berwanger, F. Huber, F. Stilp, and F. J. Giessibl, Lateral manipulation of single iron adatoms by means of combined atomic force and scanning tunneling microscopy using CO-terminated tips, *Phys. Rev. B* **98**, 195409 (2018).
- [51] J. Brand, N. Néel, and J. Kröger, Moving atoms on surfaces: Impact of external parameters on required lateral force, *Phys. Rev. B* **98**, 235420 (2018).
- [52] Y. Zhang, D. J. Trainer, B. Narayanan, Y. Li, A. T. Ngo, S. Khadka, A. Neogi, B. Fisher, L. A. Curtiss, S. K. R. S. Sankaranarayanan *et al.*, One-dimensional lateral force anisotropy at the atomic scale in sliding single molecules on a surface, *Nano Lett.* **21**, 6391 (2021).
- [53] D. Yesilpinar, B. S. Lammers, A. Timmer, Z. X. Hu, W. Ji, S. Amirjalayer, H. Fuchs, and H. Monig, Mechanical and chemical interactions in atomically defined contacts, *Small* **17**, 2101637 (2021).
- [54] Y. Adachi, Y. Sugawara, and Y. J. Li, Probing CO on a rutile TiO₂(110) surface using atomic force microscopy and Kelvin probe force microscopy, *Nano Res.* **15**, 1909 (2022).
- [55] M. F. Crommie, C. P. Lutz, and D. M. Eigler, Confinement of electrons to quantum corrals on a metal-surface, *Science* **262**, 218 (1993).
- [56] A. J. Heinrich, C. P. Lutz, J. A. Gupta, and D. M. Eigler, Molecule cascades, *Science* **298**, 1381 (2002).
- [57] K. K. Gomes, W. Mar, W. Ko, F. Guinea, and H. C. Manoharan, Designer Dirac fermions and topological phases in molecular graphene, *Nature (London)* **483**, 306 (2012).
- [58] L. Gross, F. Mohn, N. Moll, P. Liljeroth, and G. Meyer, The chemical structure of a molecule resolved by atomic force microscopy, *Science* **325**, 1110 (2009).
- [59] M. Neu, N. Moll, L. Gross, G. Meyer, F. J. Giessibl, and J. Repp, Image correction for atomic force microscopy images with functionalized tips, *Phys. Rev. B* **89**, 205407 (2014).
- [60] C. L. Chiang, C. Xu, Z. Han, and W. Ho, Real-space imaging of molecular structure and chemical bonding by single-molecule inelastic tunneling probe, *Science* **344**, 885 (2014).

- [61] P. Hapala, R. Temirov, F. S. Tautz, and P. Jelinek, Origin of High-Resolution IETS-STM Images of Organic Molecules with Functionalized Tips, *Phys. Rev. Lett.* **113**, 226101 (2014).
- [62] M. Corso, M. Ondracek, C. Lotze, P. Hapala, K. J. Franke, P. Jelinek, and J. I. Pascual, Charge Redistribution and Transport in Molecular Contacts, *Phys. Rev. Lett.* **115**, 136101 (2015).
- [63] B. de la Torre, M. Svec, G. Foti, O. Krejci, P. Hapala, A. Garcia-Lekue, T. Frederiksen, R. Zboril, A. Arnau, H. Vazquez *et al.*, Submolecular Resolution by Variation of the Inelastic Electron Tunneling Spectroscopy Amplitude and its Relation to the AFM/STM Signal, *Phys. Rev. Lett.* **119**, 166001 (2017).
- [64] F. Huber, J. Berwanger, S. Polesya, S. Mankovsky, H. Ebert, and F. J. Giessibl, Chemical bond formation showing a transition from physisorption to chemisorption, *Science* **366**, 235 (2019).
- [65] F. Stilp, A. Berezuk, J. Berwanger, N. Mundigl, K. Richter, and F. J. Giessibl, Very weak bonds to artificial atoms formed by quantum corrals, *Science* **372**, 1196 (2021).
- [66] T. Komeda, Y. Kim, M. Kawai, B. N. J. Persson, and H. Ueba, Lateral hopping of molecules induced by excitation of internal vibration mode, *Science* **295**, 2055 (2002).
- [67] J. I. Pascual, N. Lorente, Z. Song, H. Conrad, and H. P. Rust, Selectivity in vibrationally mediated single-molecule chemistry, *Nature (London)* **423**, 525 (2003).
- [68] N. Lorente and H. Ueba, CO dynamics induced by tunneling electrons: Differences on Cu(110) and Ag(110), *Eur. Phys. J. D* **35**, 341 (2005).
- [69] Y. Kim, K. Motobayashi, T. Frederiksen, H. Ueba, and M. Kawai, Action spectroscopy for single-molecule reactions—Experiments and theory, *Prog. Surf. Sci.* **90**, 85 (2015).
- [70] J. N. Ladenthin, T. Frederiksen, M. Persson, J. C. Sharp, S. Gawinkowski, J. Waluk, and T. Kumagai, Force-induced tautomerization in a single molecule, *Nature Chem.* **8**, 935 (2016).
- [71] H. Okuyama, H. So, S. Hatta, T. Frederiksen, and T. Aruga, Effect of adsorbates on single-molecule junction conductance, *Surf. Sci.* **678**, 169 (2018).
- [72] A. Shiotari, T. Odani, and Y. Sugimoto, Torque-Induced Change in Configuration of a Single NO Molecule on Cu(110), *Phys. Rev. Lett.* **121**, 116101 (2018).
- [73] A. J. Weymouth, E. Riegel, B. Simmet, O. Gretz, and F. J. Giessibl, Lateral force microscopy reveals the energy barrier of a molecular switch, *ACS Nano* **15**, 3264 (2021).
- [74] N. Okabayashi, T. Frederiksen, A. Liebig, and F. J. Giessibl, companion paper, Dynamic Friction Unraveled by Observing an Unexpected Intermediate State in Controlled Molecular Manipulation, *Phys. Rev. Lett.* **131**, 148001 (2023).
- [75] F. J. Giessibl, Atomic resolution on Si(111)-(7 × 7) by non-contact atomic force microscopy with a force sensor based on a quartz tuning fork, *Appl. Phys. Lett.* **76**, 1470 (2000).
- [76] J. E. Sader and S. P. Jarvis, Accurate formulas for interaction force and energy in frequency modulation force spectroscopy, *Appl. Phys. Lett.* **84**, 1801 (2004).
- [77] B. J. Albers, M. Liebmann, T. C. Schwendemann, M. Z. Baykara, M. Heyde, M. Salmeron, E. I. Altman, and U. D. Schwarz, Combined low-temperature scanning tunneling/atomic force microscope for atomic resolution imaging and site-specific force spectroscopy, *Rev. Sci. Instrum.* **79**, 033704 (2008).
- [78] Z. Majzik, M. Setvin, A. Bettac, A. Feltz, V. Chab, and P. Jelinek, Simultaneous current, force and dissipation measurements on the Si(111) 7 × 7 surface with an optimized qPlus AFM/STM technique, *Beilstein J. Nanotechnol.* **3**, 249 (2012).
- [79] A. Peronio, N. Okabayashi, F. Griesbeck, and F. Giessibl, Radio frequency filter for an enhanced resolution of inelastic electron tunneling spectroscopy in a combined scanning tunneling- and atomic force microscope, *Rev. Sci. Instrum.* **90**, 123104 (2019).
- [80] J. Welker and F. J. Giessibl, Revealing the angular symmetry of chemical bonds by atomic force microscopy, *Science* **336**, 444 (2012).
- [81] N. Okabayashi, A. Gustafsson, A. Peronio, M. Paulsson, T. Arai, and F. J. Giessibl, Influence of atomic tip structure on the intensity of inelastic tunneling spectroscopy data analyzed by combined scanning tunneling spectroscopy, force microscopy, and density functional theory, *Phys. Rev. B* **93**, 165415 (2016).
- [82] G. Kresse and J. Furthmüller, Efficient iterative schemes for ab initio total-energy calculations using a plane-wave basis set, *Phys. Rev. B* **54**, 11169 (1996).
- [83] G. Kresse and D. Joubert, From ultrasoft pseudopotentials to the projector augmented-wave method, *Phys. Rev. B* **59**, 1758 (1999).
- [84] N. Okabayashi, T. Frederiksen, A. Liebig, and F. J. Giessibl, Dataset for “Energy dissipation of a carbon monoxide molecule manipulated using a metallic tip on copper surfaces”, doi:10.5281/zenodo.8261814 (2023).
- [85] J. Klimeš, D. R. Bowler, and A. Michaelides, Van der Waals density functionals applied to solids, *Phys. Rev. B* **83**, 195131 (2011).
- [86] G. Mills, H. Jonsson, and G. K. Schenter, Reversible work transition-state theory—Application to dissociative adsorption of hydrogen, *Surf. Sci.* **324**, 305 (1995).
- [87] M.-L. Bocquet and P. Sautet, STM and chemistry: A qualitative molecular orbital understanding of the image of CO on a Pt surface, *Surf. Sci.* **360**, 128 (1996).
- [88] J. A. Nieminen, E. Niemi, and K. H. Rieder, Interference between competing tunneling channels and chemical resolution of STM, *Surf. Sci.* **552**, L47 (2004).
- [89] G. Teobaldi, M. Penalba, A. Arnau, N. Lorente, and W. A. Hofer, Including the probe tip in theoretical models of inelastic scanning tunneling spectroscopy: CO on Cu(100), *Phys. Rev. B* **76**, 235407 (2007).
- [90] A. Gustafsson, N. Okabayashi, A. Peronio, F. J. Giessibl, and M. Paulsson, Analysis of STM images with pure and CO-functionalized tips: A first-principles and experimental study, *Phys. Rev. B* **96**, 085415 (2017).
- [91] G. Czap, Z. M. Han, P. J. Wagner, and W. Ho, Detection and Characterization of Anharmonic Overtone Vibrations of Single Molecules on a Metal Surface, *Phys. Rev. Lett.* **122**, 106801 (2019).
- [92] N. Néel and J. Kröger, Atomic force extrema induced by the bending of a CO-functionalized probe, *Nano Lett.* **21**, 2318 (2021).
- [93] B. G. Briner, M. Doering, H. P. Rust, and A. M. Bradshaw, Microscopic molecular diffusion enhanced by adsorbate interactions, *Science* **278**, 257 (1997).
- [94] J. Ahner, D. Mocuta, R. D. Ramsier, and J. T. Yates, Adsorbate-adsorbate repulsions—The coverage dependence of the adsorption structure of CO on Cu(110) as studied by electron-stimulated desorption ion angular distribution, *J. Chem. Phys.* **105**, 6553 (1996).